Journal of Inorganic Biochemistry 198 (2019) 110750

Contents lists available at ScienceDirect

Journal of Inorganic Biochemistry

journal homepage: www.elsevier.com/locate/jinorgbio

Bi- and trinuclear copper(I) compounds of 2,2,5,5-tetramethylimidazolidine-4-thione and 1,2-bis(diphenylphosphano)ethane: Synthesis, crystal structures, *in vitro* and *in silico* study of antibacterial activity and interaction with DNA and albumins

Despoina Anastasiadou[a], George Psomas[a,*], Stavros Kalogiannis[b], George Geromichalos[a], Antonios G. Hatzidimitriou[a], Paraskevas Aslanidis[a,*]

[a] Laboratory of Inorganic Chemistry, Department of Chemistry, Aristotle University of Thessaloniki, Thessaloniki 54124, Greece
[b] Department of Nutrition and Dietetics, Faculty of Agriculture, Food Technology and Nutrition, Alexander Technological Educational Institution, Sindos, Thessaloniki, Greece

ARTICLE INFO

Keywords:
Copper(I)
2,2,5,5-tetramethylimidazolidine-4-thione
Antibacterial activity
Interaction with DNA
Binding with albumins
In silico molecular docking

ABSTRACT

Herein we report on the synthesis, molecular structures, DNA-binding properties and antibacterial activity of four new copper(I) mixed-ligand complexes obtained by reacting copper(I) halides or $[Cu(CH_3CN)_4](BF_4)$ with 1,2-bis(diphenylphosphano)ethane (dppe) and 2,2,5,5-tetramethylimidazolidine-4-thione (tmimdtH). Depending on the nature of the halide, the resulting compounds adopt two different structural motifs. Thus, using CuCl or CuBr, doubly dppe-bridged symmetrical dimmers of type $[(\kappa\text{-S-tmimdtH})XCu(\mu\text{-dppe})_2CuX(\kappa\text{-S-tmimdtH})]$ are formed, while in the case of CuI, a rare example of a trinuclear complex was isolated, in which the Cu atom of a CuI(tmimdtH) moiety is linked by two bridging dppe units with the two Cu atoms of a cluster-type Cu_2I_2(dppe) core. On the other hand, $[Cu(CH_3CN)_4](BF_4)$ reacts with the anion of tmimdtH in the presence of dppe to form a binuclear complex consisting of two (dppe)Cu(tmimdt) units linked together by the P atoms of a dppe bridging ligand. The complexes show significant *in vitro* antibacterial activity against certain bacterial strains. An intercalative mode is suggested as the most probable interaction fashion of the compounds with calf-thymus (CT) DNA, monitored directly *via* UV–vis spectroscopy, DNA-viscosity measurements and indirectly *via* their competition with ethidium bromide for DNA as studied by fluorescence emission spectroscopy. The binding of the complexes to human (HSA) and bovine serum albumin (BSA) is tight. In order to explain the described *in vitro* activity of the compounds, we adopted molecular docking studies on the crystal structure of HSA, BSA, CT DNA and DNA-gyrase.

1. Introduction

Heterocyclic thiones constitute an extended family of versatile S,N-donor ligands incorporating soft and hard coordination sites, thus, being capable of forming complexes with virtually any transition metal [1–3]. In this context, particularly intense research activity was noted in the area of complexes of monovalent group 11 metal ions, which are characterized by a rich structural diversity. Long-lasting relevant research in our laboratory focuses on thione-ligated copper(I) and silver (I) complexes containing tertiary aryl phosphanes and diphosphanes as bulky auxiliary π-acceptor ligands. While the initial goal of our investigations was to recognize the factors responsible for the stoichiometric and structural preferences of the resulting compounds [4], meanwhile we realized that many of these compounds show particularly interesting biological activity, so we decided to turn our attention to this direction, searching for possible relationships between structure and bioactivity.

As an essential trace element, copper is required as cofactor for the redox-active centers of various enzymes and proteins involved in a number of cellular processes such as immune function [5], respiration [6], and angiogenesis [7]. Redox-active copper centers are also found in some low molecular weight copper-rich metallothioneins, where the metal is bound to cysteine, forming stable polynuclear copper(I)-thiolate clusters. Understanding the chemistry and biology behind the physiological function of those copper-thioneins requires well-defined relevant structural information which could arise as the result of a

* Corresponding authors.
E-mail addresses: gepsomas@chem.auth.gr (G. Psomas), aslanidi@chem.auth.gr (P. Aslanidis).

https://doi.org/10.1016/j.jinorgbio.2019.110750
Received 23 April 2019; Received in revised form 4 June 2019; Accepted 5 June 2019
Available online 08 June 2019
0162-0134/

thorough study of the coordination behavior of copper in related low nuclearity model complexes. In this regard, heterocyclic thione ligands appear to be a useful and promising starting point for modeling the cysteine bonding, and this is one of the main reasons for the intense research interest in their coordination chemistry over the last decades.

Bioactive copper complexes are currently under investigation for their potential use as antimicrobial [8,9], anti-inflammatory [10,11] and antitumor [12–14] agents. Relevant research in our laboratory has focused on copper(I) halide and silver(I) complexes of *N*-methylbenzothiazole-2-thione which showed significant antibacterial activity [15–18].

DNA is recognized as one of the common biological targets of anticancer drugs, since one of the main mechanisms of action of the anticancer drugs is the damage of DNA [19]. Bacterial DNA-gyrase is a topoisomerase type II enzyme that has attracted attention since its discovery in 1976, when it was first isolated from *Escherichia coli* [20]. DNA-gyrase catalyzes changes in DNA topology by breaking and rejoining double stranded DNA, introducing negative supercoils of the closed-circular DNA in front of the replication fork [21]. As this function is essential for DNA replication and transcription, DNA-gyrase is really a suitable target for antibacterial agents, since its blocking induces bacterial cell death. Serum albumin (SA) is a multifunctional protein with extraordinary ligand binding capacity, making it a transporter molecule for a diverse range of metabolites, drugs, nutrients, metals and other molecules. Due to its ligand binding properties, albumins have wide clinical, pharmaceutical, and biochemical applications [22,23].

Continuing our investigations on the structural and biological properties of heteroleptic thione/phosphane containing coinage metal complexes, we herein report the structural and spectroscopic characteristics of four new neutral copper(I) complexes bearing the virtually unexplored 2,2,5,5-tetramethyl-imidazolidine-4-thione (tmimdtH, Scheme 1) and 1,2-bis(diphenylphosphano)ethane (dppe) as ligands, as well as the results on their antibacterial activity against several Gram-positive and Gram-negative microorganisms. Further, we present the results of the *in vitro* interaction of these complexes with calf-thymus (CT) DNA and bovine (BSA) and human serum albumin (HSA) by diverse techniques. *In silico* approaches with the employment of molecular docking simulations on the crystal structure of CT DNA and the target protein DNA-gyrase were employed to elucidate the capacity of compounds **1–4** to act as antibacterial agents, suggesting a mode of action of these compounds. Further, *in silico* approaches with the employment of molecular docking were adopted in an attempt to provide information for the understanding of the ability of the compounds in transportation through HSA and BSA and, thus, possible interaction with other protein targets involved in various diseases and especially, cancer.

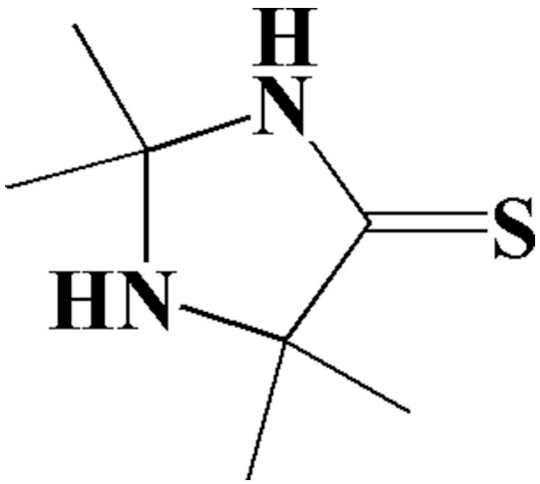

Scheme 1. The heterocyclic thioamide tmimdtH used as ligand.

2. Experimental

2.1. General procedures and chemicals

All manipulations were carried out under atmospheric conditions, unless otherwise mentioned. Solvents were purified according to established methods and allowed to stand over molecular sieves for 24 h. Copper(I) halides, 2,2,5,5-tetramethylimidazolidine-4-thione (tmimdtH), 1,2-bis(diphenylphosphano)ethane (dppe), CT DNA, ethidium bromide (EB), HSA, BSA, NaCl and trisodium citrate were obtained from commercial sources and used without any further purification. $[Cu(CH_3CN)_4](BF_4)$ was prepared according to a procedure described in the literature [24].

DNA stock solution was prepared by dilution of CT DNA to buffer (containing 15 mM trisodium citrate and 150 mM NaCl at pH 7.0) followed by stirring for three days and kept at 4 °C for no longer than ten days. This solution of CT DNA gave a ratio of UV absorbance at 260 and 280 nm (A_{260}/A_{280}) of ~1.90, indicating that the DNA was sufficiently free of protein contamination [25]. The DNA concentration was determined by the UV absorbance at 260 nm after 1:20 dilution using $\varepsilon = 6600\ M^{-1}\ cm^{-1}$ [26].

2.2. Instrumentation

Infrared spectra (IR) in the region of 4000–200 cm^{-1} were recorded in KBr discs with a Nicolet FT-IR 6700 spectrophotometer. UV–visible (UV–vis) spectra were recorded as nujol mulls and in acetonitrile or DMSO solution at concentrations in the range 10^{-5}–10^{-3} M on a Hitachi U-2001 dual beam spectrophotometer. Emission/excitation spectra of the solid samples and in solution were recorded on a Hitachi F-7000 fluorescence spectrophotometer. Viscosity experiments were carried out using an ALPHA L Fungilab rotational viscometer equipped with an 18 mL LCP spindle.

2.3. X-ray crystal structure determinations

Single-crystals of all compounds, suitable for X-ray crystallographic analysis, were mounted on thin glass fibers with the aid of an epoxy resin. X-ray diffraction data were collected on a Bruker Apex II CCD area-detector diffractometer, equipped with a Mo Ka (λ = 0.71070 Å) sealed tube source, at 295 K, using the φ and ω scans technique. The program Apex2 (Bruker AXS, 2006) was used in data collection, cell refinement, and data reduction [27]. Structures were solved with Superflip [28] and refined with full-matrix least-squares using the program Crystals [29]. Anisotropic displacement parameters were applied to all non-hydrogen atoms, while hydrogen atoms were generated geometrically and refined using a riding mode to the pivot atom. Details of crystal data and structure refinement parameters are shown in Table S1. Plots of the molecular structures of all compounds were obtained by using the program Mercury [30].

2.4. Syntheses

2.4.1. General procedure for the syntheses of compounds 1–3

To a solution of 0.5 mmol of copper(I) halide (0.050 g for CuCl, 0.072 g for CuBr, 0,095 g for CuI) in 40 mL of dry acetone, a solution of dppe (0.5 mmol, 0.199 g) in 40 mL acetone was added dropwise. After stirring the resulting clear mixture at 50 °C for 1 h, a 30 mL solution of tmimdtH (0.5 mmol, 0.079 g) in acetone was added dropwise and the reaction mixture was further stirred at 50 °C for 2 h and then it was filtered in order to remove a small amount of a pale yellow solid. The filtrate was set aside to evaporate slowly at room temperature and over a period of a few days, crystals were formed, which were filtered off and dried under vacuum.

2.4.1.1. [(κ-S-tmimdtH)ClCu(μ-dppe)$_2$CuCl(κ-S-tmimdtH)],

(1). Colorless crystals, m.p. 210 °C. Anal. Calc. for [(tmimdtH)CuCl(dppe)]$_2$ $C_{66}H_{76}N_4Cl_2Cu_2P_4S_2$ (MW = 1311.38): C 60.45, H 5.84, N 4.27; found C 60.62, H 5.89, N 4.22. FTIR (KBr, cm^{-1}): 3048 m, 2973 s, 2918 m, 1571 m, 1526vs, 1432s, 1367 m, 1383s, 1369s, 1189s, 1071s, 1098s, 1062vs, 888 m, 750 s, 738vs, 723vs, 691vs, 506vs, 481vs, 465 s. UV–vis (λ_{max}, log ε), in CH_3CN: 221 (5.12), 265 (4.52); in DMSO: 264.5 (4.94), 271 (4.89).

2.4.1.2. [(κ-S-tmimdtH)BrCu(μ-dppe)$_2$CuBr(κ-S-tmimdtH)], ***2***. Colorless crystals, m.p. 238–245 °C (decomp.). Anal. Calc. for [(tmimdtH)CuBr(dppe)]$_2$ $C_{66}H_{76}N_4Br_2Cu_2P_4S_2$ (MW = 1400.28): C 56.61, H 5.47, N 4.00; found C 56.77, H 5.56, N 3.97. FTIR (KBr, cm^{-1}): 3050 m, 2977 s, 2920 m, 1570 m, 1521vs, 1433vs, 1382s, 1368s, 1187s, 1097s, 1060vs, 887 s, 760 s, 724vs, 691vs, 506vs, 483vs, 464 s. UV–vis (λ_{max}, log ε), in CH_3CN: 220 (5.11), 266 (4.75); in DMSO: 265 sh (4.98), 271 (4.93).

2.4.1.3. [I(κ-S-tmimdtH)Cu(μ-dppe)$_2${Cu(μ-dppe)(μ-I)$_2$Cu}], ***3***. Colorless crystals, m.p. 204 °C. Anal. Calc. for [(tmimdtH)Cu_3I_3(dppe)$_3$].$CH_3C(O)CH_3$ $C_{88}H_{92}N_2Cu_3I_3N_2OP_6S$ (MW = 1982.97): C 53.30, H 4.68, N 1.41; found C 53.14, H 4.63, N 1.44. FTIR (KBr, cm^{-1}): 3049 m, 1571m68s, 1519s, 1483s, 1435vs, 1307 m, 1177s, 1098vs, 1026vs, 883 m, 739vs, 693vs, 512vs, 480vs. UV–vis (λ_{max}, log ε), in CH_3CN: 228 (4.76), 244 (4.70); in DMSO: 264.5 (4.12), 271 (4.06).

2.4.2. Synthesis of [(dppe)(κ-S-tmimdt)Cu(μ$_2$-dppe)Cu(κ-S-tmimdt)(dppe)], ***4***

Solid dppe (1.0 mmol, 0.398 g) was added to a solution of [Cu$(CH_3CN)_4$](BF_4) (0. 157 g, 0.5 mmol) in 30 mL of dry acetonitrile and the mixture was stirred at 50 °C for 1 h. To the resulting clear mixture, a solution of tmimdtH (0.5 mmol, 0.079 g) that had previously been deprotonated by addition of 1.0 mL of 0.5 M KOH in methanol, was added dropwise. The light yellow reaction mixture was further stirred at 50 °C for 2 h and then it was filtered in order to remove a small amount of insoluble material. The solution was set aside in dark to evaporate slowly at room temperature. Over a period of a few days a crystalline solid was obtained, which was filtered off and collected. Colorless crystals, m.p. 195 °C. Anal. Calc. for [(tmimdt)$_2Cu_2$(dppe)$_3$].(1/2)CH_3COCH_3.$2H_2O$ $C_{83.5}H_{105}N_4Cu_2O_{2.5}P_6S_2$ (MW = 1701.95): C 65.98, H 6.22, N 3.29; found C 65.79, H 6.18, N 3.33. FTIR (KBr, cm^{-1}): 3048 s, 2968 s, 2923 m, 1585vs, 1540vs, 1482vs, 1434vs, 1370s, 1383s, 1357s, 1164s, 1097vs, 1033vs, 997 s, 872 m, 743vs, 695vs, 510vs, 478 s. UV–vis (λ_{max}, log ε), in CH_3CN: 221 (4.98), 266 (4.62); in DMSO: 271 (4.90).

2.5. Antibacterial activity

The antimicrobial activity of complexes **1–4** was evaluated by determining their respective IC_{50} and the MIC values towards two Gram-(−) (*Escherichia coli* NCTC 29212 (*E. coli*) and *Xanthomonas campestris* ATCC 1395 (*X. campestris*)) and two Gram-(+) (*Staphylococcus aureus* ATCC 6538 (*S. aureus*) and *Bacillus subtilis* ATCC 6633 (*B. subtilis*)) bacterial species. Cultures of these microbial strains were grown on a rich selective agar medium and stored at 4 °C. The selective media used were Nutrient Agar or Broth for *B. subtilis* and *S. aureus*, Yeast Mold Agar or Broth for *X. campestris* and Luria Agar or Broth for *E. coli*. Cells picked from the surface of the stored cultures were used to initiate liquid pre-cultures of the same selective medium at an initial turbidity of roughly 1 McFarland unit. Pre-cultures were incubated for 24 h in a rotary shaking incubator and subsequently they were used to inoculate the test cultures used for the determination of MIC at an initial turbidity of 0.5 McFarland units. The test cultures consisted of Mueller-Hinton broth (Deben Diagnostics Ltd) containing different concentrations of the compounds. Different concentrations were achieved as follows: the compounds were freshly dissolved in DMSO to a concentration of 1 mg mL^{-1} and they were diluted with DMSO, using the method of progressive double dilution. Therefore, working solutions with decreasing concentrations of the compounds under investigation were achieved. The working solutions were subsequently diluted to the final desired concentration by addition to the growth medium at a proportion of 2:98. In order to achieve higher concentrations of the compounds under investigation two additional cultures were grown in triplicate containing the solution of the highest concentration and growth medium at proportions 5:95 and 10:90 respectively. Growth in these cultures was compared to cultures containing only the solvent DMSO at equal proportions, as reference blank cultures. MIC values were determined as the lowest concentrations of the tested compounds that inhibited visible growth of each respective organism after a 24 h incubation [31]. Bacterial growth was determined by measuring the turbidity of appropriately diluted cultures at 600 nm with reference to equally diluted sterile growth medium and the inhibition achieved was calculated by comparing the turbidity of each culture to the average of the turbidity of three non-inhibited cultures. All test cultures were grown in triplicates and for the determination of MIC, growth had to be inhibited in at least two cultures of the triplicate. The half-maximal inhibitory concentration (IC_{50}) values were calculated based on the best linear fit of the cultures absorbance grown in the presence of at least three concentrations of the inhibiting factor. Incubation temperature at all stages was 37 °C except for *X. campestris* that was cultivated at 28 °C [32].

2.6. Binding studies with biomolecules

The complexes **1–4** exhibit low solubility in water, therefore the compounds were initially dissolved in DMSO (1 mM) during the *in vitro* biological experiments, *i.e.* interaction with DNA or albumins. Mixing of such solutions with the aqueous buffer solutions of DNA or albumins used in the studies never exceeded 5% DMSO (v/v) in the final solution. All studies were performed at room temperature. Control experiments with DMSO were performed and no changes in the spectra of the CT DNA were observed.

2.6.1. Interaction with CT DNA

2.6.1.1. DNA-binding studied by UV–vis spectroscopy. The interaction of complexes **1–4** with CT DNA was monitored by UV–vis spectroscopy in order to investigate the possible mode of their binding to CT DNA and to calculate the corresponding DNA-binding constants (K_b). The UV spectra of CT DNA were recorded for a constant DNA concentration (1.2–1.4 × 10^{-4} M) in the presence of each complex at diverse [complex]/[DNA] mixing ratios (=*r*). Furthermore, the UV–vis spectra of the complexes were recorded for a constant concentration (2 × 10^{-4}–1 × 10^{-4} M) in the presence of increasing amounts of CT DNA at diverse [DNA]/[complex] mixing ratios (=*r*'). The values of K_b (in M^{-1}) were obtained by monitoring the changes in the absorbance at the corresponding λ_{max} with increasing concentrations of CT DNA and were calculated by the ratio of slope to the y intercept in plots [DNA]/(ε_A-ε_f) *versus* [DNA], according to the Wolfe-Shimer equation (Eq. (S1)) [33].

2.6.1.2. DNA-viscosity measurements. The viscosity of DNA ([DNA] = 0.1 mM) in buffer solution (150 mM NaCl and 15 mM trisodium citrate at pH 7.0) was measured in the presence of increasing amounts of complexes **1–4** (up to the *r* value = 0.35). All measurements were performed at room temperature. The obtained data are presented as $(\eta/\eta_0)^{1/3}$ *versus r*, where η is the viscosity of DNA in the presence of the complex, and η_0 is the viscosity of DNA alone in buffer solution.

2.6.1.3. EB-competition studied by fluorescence emission spectroscopy. The competition of complexes **1–4** with EB was investigated by fluorescence emission spectroscopy in order to examine whether the complexes can displace EB from its DNA-EB conjugate. The DNA-EB conjugate was prepared by adding 20 μM EB and 26 μM CT DNA in buffer (150 mM

NaCl and 15 mM trisodium citrate at pH 7.0). The possible intercalating effect of the complexes was studied by adding stepwise a certain amount of a solution of the compound into a solution of the DNA-EB conjugate. The influence of the addition of each complex into the DNA-EB solution was obtained by monitoring the changes of fluorescence emission spectra with excitation wavelength (λ_{ex}) at 540 nm [34]. The compounds did not show any fluorescence emission bands at room temperature in solution or in the presence of DNA or EB under the same experimental conditions (λ_{ex} = 540 nm); therefore, the observed quenching may be attributed to the displacement of EB from its EB-DNA conjugate. The Stern-Volmer constant (K_{SV}, in M^{-1}) is usually used to evaluate the quenching efficiency for each compound according to the Stern-Volmer equation (Eq. (S2)) [34]. Taking τ_o = 23 ns as the fluorescence lifetime of the EB-DNA system [35], the quenching constants (k_q, $M^{-1}s^{-1}$) of the complexes were calculated according to Eq. (S3).

2.6.2. Albumin-binding studies

The albumin-binding studies were performed by tryptophan fluorescence quenching emission experiments using BSA (3 μM) or HSA (3 μM) in buffer solution (containing 15 mM trisodium citrate and 150 mM NaCl at pH 7.0). The quenching of the emission intensity of tryptophan residues of BSA or HSA was monitored using the compounds as quenchers with increasing concentrations [34]. The fluorescence emission spectra were recorded in the range 300–500 nm with λ_{ex} = 295 nm. The free compounds did not exhibit any significant emission band when the fluorescence emission spectra were recorded under the same experimental conditions, *i.e.* λ_{ex} = 295 nm. Furthermore, control experiments with DMSO were performed and no changes (*i.e.* quenching) in the fluorescence emission spectra of the albumins were observed. The influence of the inner-filter effect [36] on the measurements was evaluated by Eq. (S4). The Stern-Volmer and Scatchard equations (Eqs. (S2), (S3) and (S5)) [37] and graphs were used in order to study the interaction of each quencher with serum albumins and to calculate the Stern-Volmer constant K_{SV} (in M^{-1}), the quenching constant k_q (in $M^{-1}s^{-1}$), the SA-binding constant K (in M^{-1}) and the number of binding sites per albumin.

2.7. In silico computational methods (molecular modeling and docking calculations)

The *in silico* predictive tools that have been employed to study the properties of the compounds to act as anticancer and/or antibacterial agents are Spartan ′14, v.1.1.4, BioMedCACche, UCSF Chimera, YASARA and Schrödinger molecular modeling software.

Molecular models of compounds **1–4** were built in 3D coordinates and their best, most stable (lowest energy) conformation was detected by geometrical optimization of each structure in the gas phase, as implemented in the Spartan ′14 Molecular Modeling program suite [38]. The structure of each molecule was initially optimized (*via* energy minimization) by conformational search using the Monte Carlo method with the MMFF94 molecular mechanics model, included in the Spartan ′14 program suite. Geometry optimization (leading to the most stable conformer with the lowest energy) was accomplished *via* quantum-chemical calculations by utilizing the *ab initio* Hartree-Fock method with a 6-31G* basis set.

The molecular docking study was carried out on the crystal structure of HSA, BSA, DNA gyrase and CT DNA dodecamer d (CpGpCpGpApApTpTpCpGpCpG) target macromolecules (Protein Data Bank, PDB entry codes 2BXG, 4OR0, 1KZN and 1BNA, respectively), to investigate the effect of the synthesized compounds on these targets. X-ray structures of the (i) HSA protein in complex with bound co-crystallized drug ibuprofen (IBP, 2-(4-isobutylphenyl)propionic acid) [39], (ii) BSA protein in complex with bound co-crystallized drug naproxen (NPS, (*S*)-2-(6-methoxynaphthalen-2-yl)propanoic acid) [40] (iii) DNA-gyrase in complex with bound co-crystallized drug chlorobiocin (CBN) [41] and (iv) synthetic CT DNA-dodecamer [42] were obtained from the Brookhaven Protein Data Bank (operated by the Research Collaboratory for Structural Bioinformatics, RCSB) [43–45]. The chosen crystal structures of HSA, BSA and DNA-gyrase has been refined at 2.70 Å, 2.58 Å and 2.30 Å resolution, conjugated with IBP, NPS and CBN, respectively, while the crystal structure of the synthetic DNA-dodecamer has been refined at 1.9 Å resolution. For the docking calculations on HSA and BSA, only the A chains of the proteins were used since chain B is replicate, with IBP and NPS bound at the same ligand binding site among the chains. For this reason, from corresponding PDB files the data for chain B and also the data of the drug referring to this chain were deleted.

The molecular docking simulation was performed in project leader of BioMedCACche 7.5 computer-aided chemistry software package, which is part of the CACche package (CACche WorkSystem Pro version 7.5.0.85, Fujitsu Co. Ltd., Tokyo, Japan). BioMedCACche engages a stochastic optimization method to enhance the intra-molecular energy of a ligand by rotation and analyzing various orientations. BioMedCACche automates the docking of ligand into active or binding sites by using a genetic algorithm with a fast, simplified potential mean force (PMF). The potential of mean force is a knowledge-based approach that extracts pairwise atomic potentials from structure information of known protein-ligand complexes contained in the protein data bank.

Docking was carried out at full rotation allowing full flexibility for the ligand while keeping the target protein's and DNA positions fixed in space. Docking parameters involved steric scan, final search for ligand binding site and refinement of the complex. Cache docking score performs force fields which includes terms as bond stretching, angle bending, torsional, and nonbonded interactions such as van der Waals and hydrogen-bond interactions. The molecule-based scoring function is made up of four components: 1. Protein-ligand H-bond energy (external H-bond). 2. Protein-ligand van der Waals energy (external vdw). 3. Ligand internal van der Waals energy (internal vdw). 4. Ligand intramolecular H-bond energy (internal H-bond). Docking Score = S (hb_ext) + S (vdw_ext) + S (hb_int) + S (vdw_int). The produced compound-protein conjugates were ranked by the energy score, including their binding conformations. Best docked poses, with both lower binding energies and stronger interaction pattern, were derived from a number of solutions (docking results), usually with the higher ranking. A more rigorous docking function for the final pose selection/ranking of ligands (scoring procedure) was adopted for the best-scored lead compound (recalculation of the energy of the top scoring poses in order to improve the selectivity between the lead compounds). This refinement of the scoring poses was necessary in order to minimize the number of false positive and false negative ligands. Three-dimensional (3D) models of the above protein crystal structures were developed, after the deletion of the co-crystallized bound inhibitor. The final output of the docking procedure is a set of solutions (docking results) ranked according to the corresponding scoring function values, each defined by the 3D coordinates of its atoms and expressed as a PDB file.

In this study, the docking procedure with the aid of BioMedCACche was shown to accurately reproduce experimentally observed binding modes of IBU and CBN, in terms of RMSD (root-mean squared deviation). The BioMedCACche provided excellent results as low values of RMSD (best docked solutions of docking results 0.23 Å and 0.31 Å, respectively) were observed between the experimental and the best-scoring docked structures derived by superimposition of these structures (the accuracy of the docking results are good when the RMSD is mostly below 1.0 Å). The ability to accurately predict the binding conformation of the enzyme inhibitor and substrate, gave confidence that the BioMedCACche would also exhibit a similar accuracy with the investigated molecules in the study. The UCSF Chimera package (developed by the Resource for Biocomputing, Visualization, and Informatics at the University of California, San Francisco, supported by NIGMS P41-GM103311), production version 1.11, (http://www.rbvi.

ucsf.edu/chimera) [46], YASARA molecular modeling package version 19.1.27 (http://www.yasara.org) [47] and PyMol (Schrödinger, LLC. version 1.8.2.0, www.pymol.org) [48] Molecular Graphics Systems were used to visualize the molecules and analyze the results of the docking and to construct the molecular models.

3. Results and discussion

3.1. Synthesis and spectroscopic information

Compounds **1–3** are accessible *via* the direct treatment of copper(I) halides with equivalent amounts of 1,2-bis(diphenylphosphano)ethane (dppe) and 2,2,5,5-tetramethylimidazolidine-4-thione (tmimdtH) under mild conditions. In particular, in a first step, a solution of the copper halide in dry acetone is left to react with the diphosphane to form a white precipitate of the intermediate complex, which is then treated with an acetone solution containing the thione ligand. Upon completion the mixing of the components, the reaction mixture clears up, indicating that the final products are formed immediately. It should be noted that this particular 1:1:1 M ratio of the reactants used in the reactions was retained only in the case of compounds **1** and **2**, while for **3** a ratio of 3:3:1 is favored under the same experimental conditions. Preparation of the analogue halide-free neutral copper(I) complex (compound **4**) takes place by reacting equivalent amounts of $[Cu(CH_3CN)_4](BF_4)$ and dppe in acetonitrile, followed by addition of one equivalent of $tmimdt^-$ (obtained by deprotonation of the corresponding neutral thioamide by an equimolar amount of KOH solution in methanol). All the compounds, isolated in the form of crystalline solids, are air-stable both in the solid state and as solutions in CH_3CN and DMSO.

The infrared spectra of compounds **1–4**, recorded in the range 4000–200 cm^{-1} show two sets of distinct and very strong sharp bands, located in the 690–750 and 465–510 cm^{-1} regions, as well as a very strong sharp band at 1432 cm^{-1}. These bands are attributed to the diphosphane ligand and remain practically unshifted upon coordination to the metal center [49,50]. In addition, the spectra of the new complexes contain the four characteristic "thioamide bands I-IV" due to the presence of the heterocyclic thione system. These bands could be helpful in determining the coordination mode of a thione ligand. In particular, thioamide bands I and II, located in the spectrum of the free tmimdtH at 1524 and 1068 cm^{-1}, and having major contributions from δ(C—H) + δ(N—H) and ν(C═N) + ν(C—N) respectively, are not significantly affected by complexation, which is in accordance with the non-coordinating nature of the nitrogen atom. On the other hand, peaks at 1068 and 697 cm^{-1} in the spectrum of the free thione, assigned to the thioamide bands III and IV, which mainly contain contributions from ν(C═S) + ν(CN) and ν(C═S), undergo red-shifts, indicative of S-donation. In the case of compound **4,** thioamide band III appears to be much stronger red-shifted (by about 35 cm^{-1}), reflecting the existence of the thioamide unit in its deprotonated form. It is to note that evaluation of such spectra may occasionally be complicated due to accumulation of several bands of different origin in the same region. This applies especially to the shifts of thioamide band IV, which though the most relevant with regard to the ligand's coordination mode, is not recognizable in the spectra of the compounds under investigation because of its overlapping with strong neighboring phosphane absorptions.

The electronic absorption spectra of the complexes, recorded in acetonitrile at room temperature, show two intense bands in the ultraviolet region with maxima at ~220–228 and ~244–266 nm. Given that both the free ligands strongly absorb in these regions, with the absorption maxima in their spectra being located at 253 nm for the dppe and at 215 and 267 nm for tmimdtH respectively, the bands in the spectra of the complexes are most likely mixed bands. Based on literature data, the higher energy band can be attributed to intraligand $\pi \rightarrow \pi^*$ transitions on the phenyl rings of the phosphane, which contains intraligand charge-transfer excitations on the part of the thione ligand, whereby the lower energy band could be considered as a thione-originating intraligand transition which possesses some MLCT character [51,52].

3.2. X-ray structures

As with other heterocyclic thiones, coordination of tmimdtH to copper(I) is expected to occur predominantly *via* the sulfur atom of the heterocycle, something that has recently been confirmed by the crystal structures of some mononuclear complexes of formula $[CuX(PPh_3)_2(tmimdtH)]$ and [CuX(totp)(tmimdtH)] (totp = tri-o-tolylphosphane) [53]. In this study, formation of three coordinated species was attributed to the increased bulk of totp compared to PPh_3. In the present case, X-ray crystallography also shows a monodentate interaction with the metal center, whereby the observed tetrahedral coordination could also be considered as expected if one takes into account that the stereochemical requirements of the flexible diphosphane dppe closely resemble these of two PPh_3 units.

Compounds **1** and **2** crystallize both in the triclinic space group *P*-1, with one and two independent molecules, respectively, in the unit cell. ORTEP diagrams of their molecular structures are shown in Figs. 1 and 2. Both compounds adopt similar structural motifs and exhibit comparable structural characteristics. They consist of two Cu atoms, which are held together by the P atoms of two bridging dppe ligands. The slightly distorted tetrahedral environment around each Cu center is completed by the S atom of a terminally coordinated neutral thione ligand, and the respective halogen atom.

Bond angles around the Cu atoms in **1** (107.21°–114.76°) are found to be very close to the expected values of an ideal tetrahedron, whereas angular distortions in **2** are somewhat larger (102.01°–115.63°). For both compounds, the Cu—P bond distances fall in the range of 2.227–2.275 Å, which are typical for bond distances in copper(I) complexes with the same diphosphane [54,55]. The Cu—S distances differ slightly from each other [2.357 Å for **1**, and 2.385 Å for **2**], but are comparable to those found in other tetrahedral copper complexes bearing the same thioamide ligand [53]. As a general remark, it can be said that in such thione/phosphane mixed-ligand complexes, this specific bond distance is particularly sensitive to steric factors in the

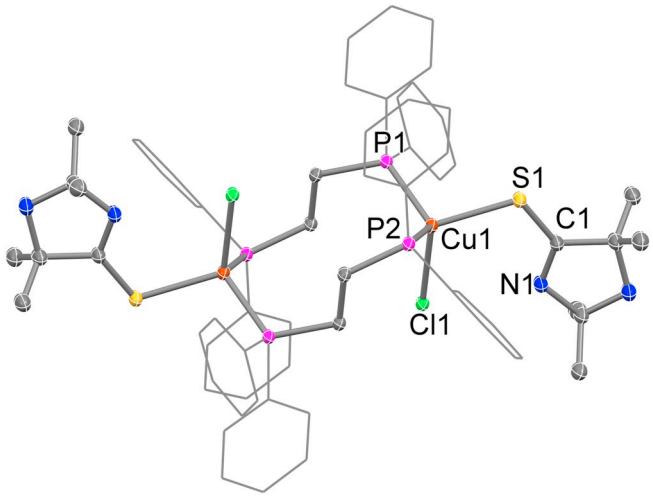

Fig. 1. Crystal structure of compound **1**. Displacement ellipsoids are shown in the 50% probability level. All hydrogen atoms have been omitted for clarity. Selected bond lengths (Å): Cu1–Cl1 = 2.4070(9), Cu1–S1 = 2.3568(10), Cu1–P1 = 2.2287(10), Cu1–$P2^i$ = 2.2266(11), S1–C1 = 1.662(4) and bond angles (°): Cl1–Cu1–S1 = 109.71(3), Cl1–Cu1–P1 = 109.15(3), Cl1–Cu1–$P2^i$ = 108.36(4), S1–Cu1–P1 = 107.56(4), S1–Cu1–$P2^i$ = 107.21(4), P1–Cu1–$P2^i$ = 114.76(4), Cu1–S1–C1 = 110.83(13). Symmetry code: (i) $-x$, $-y+1$, $-z$.

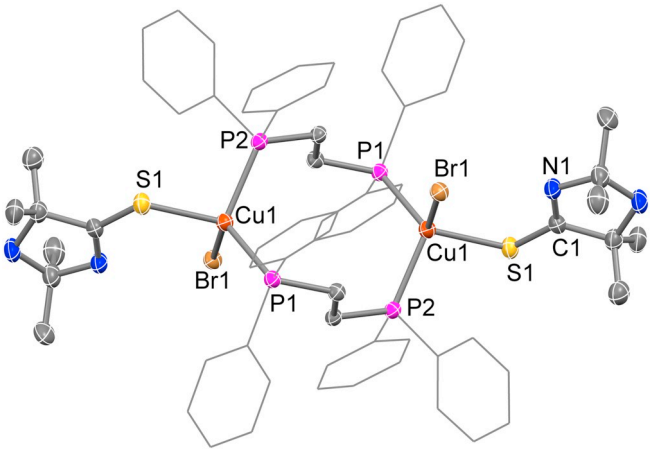

Fig. 2. Crystal structure of compound **2**. Displacement ellipsoids are shown in the 50% probability level. All hydrogen atoms have been omitted for clarity. Selected bond lengths (Å): Cu1–Br1 = 2.5226(9), Cu1–P1 = 2.2604(16), Cu1–S1 = 2.3849(16), Cu1–P2 = 2.2749(16), S1–C1 = 1.655(5) and bond angles (°): Br1–Cu1–P1 = 107.29(5), Br1–Cu1–S1 = 109.20(4), Br1–Cu1–P2 = 108.30(5), P1–Cu1–S1 = 114.16(6), P1–Cu1–P2 = 115.63(5), S1–Cu1–P2 = 102.01(6), Cu1–S1–C1 = 111.3(2).

coordination sphere. In both compounds, formation of intramolecular hydrogen-bonds between the closest NH group of the thione and the coordinated halide further contributes to the stabilization of the structures in the solid state.

Compound **3** crystallizes in the monoclinic space group $P2_1/n$, with four independent molecules in the unit cell, as well as one acetone molecule per formula unit. As shown in Fig. 3, the Cu1 atom of a CuI(tmimdtH) moiety is linked to the Cu2 and Cu3 atoms of a cluster-type Cu_2I_2(dppe) core *via* two bridging dppe units to form a quite rare example of an unsymmetrical trinuclear compound [I(κ-S-tmimdtH)Cu(μ-dppe)$_2${Cu(μ-dppe)(μ-I)$_2$Cu}] (**3**), whose composition does not reflect the initial 1:1:1 molar ratio of the reactants.

Within the bent Cu_2I_2 core with a non-bonding Cu···Cu separation of 3.267 Å and a fold angle of 30.51° along I···I, the four Cu—I bond distances are unequal to each other ranging from 2.6810 Å to 2.7558 Å.

In contrast to the abovementioned compounds **1**–**3**, in which the dppe molecules exclusively serve as bridging ligands, reaction of [Cu$(CH_3CN)_4$](BF_4) with one equivalent of dppe in acetonitrile, followed by addition of one equivalent of a thiolate ion tmimdt$^-$ (obtained by deprotonation of the corresponding neutral thione by an equimolar amount of KOH solution in methanol), results in the formation of the binuclear complex [(dppe)(κ-S-tmimdt)Cu(μ-dppe)Cu(κ-S-tmimdt)(dppe)] (compound **4**), which contains one bridging and two chelating dppe units. Product formation in this case favors a Cu/dppe/thiolate ratio of 2:3:2 over the 1:1:1 molar ratio of the reactants used. However, this particular structural type seems to be very common among the copper(I)/dppe complexes reported in the literature [56–60].

Compound **4** crystallizes in the triclinic space group P-1 with two similar, but not identical molecules per unit cell. As these two molecules do not differ significantly in their structural parameters, only one of them is discussed. Furthermore, there are water and acetone solvent molecules present in the lattice. In the centrosymmetric molecule, two (dppe)Cu(κ-S-tmimdt) units are bridged by an additional dppe ligand (Fig. 4), which results in a distorted P_3S tetrahedral coordination environment for each copper center. The bite angle of 89.52° and the Cu—P bond distances of the chelating dppe units (2.284 and 2.342 Å) fall in the range of values previously reported for analogous complexes [54,61–63]. Compared to the corresponding bond distances in **1**–**3**, the Cu—S distance in **4** is clearly shorter, while the S—C bond distance appears slightly longer, indicating the presence of a coordinated thiolate.

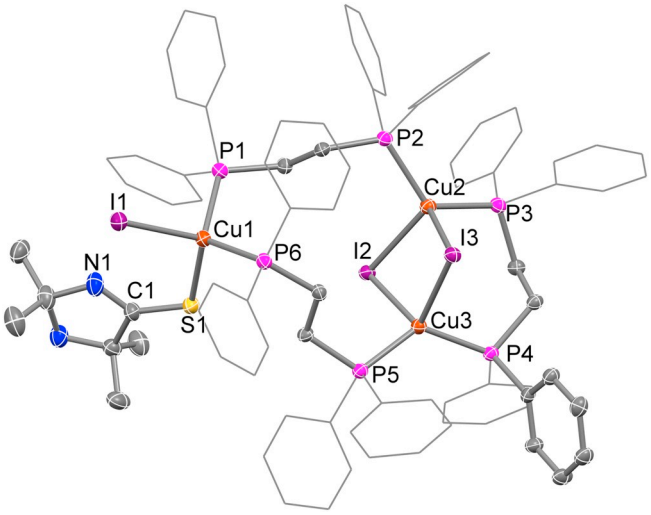

Fig. 3. Crystal structure of compound **3**. Displacement ellipsoids are shown in the 50% probability level. All hydrogen atoms have been omitted for clarity. Selected bond lengths (Å): Cu1–S1 = 2.379(2), Cu1–P1 = 2.320(2), Cu1–P6 = 2.289(2), Cu1–I1 = 2.7012(9), S1–C1 = 1.644(7), Cu2–P2 = 2.265(2), Cu2–P3 = 2.266(2), Cu2–I2 = 2.7202(8), Cu2–I3 = 2.7219(8), Cu3–P4 = 2.2565(2), Cu3–P5 = 2.250(2), Cu3–I2 = 2.6810(9), Cu3–I3 = 2.7558(8), and bond angles (°): S1–Cu1–P1 = 103.36(6), S1–Cu1–P6 = 109.01(6), S1–Cu1–I1 = 110.08(5), P1–Cu1–P6 = 117.08(6), P1–Cu1–I1 = 109.12(5), P6–Cu1–I1 = 108.04(5), Cu1–S1–C1 = 113.0(3), P2–Cu2–P3 = 125.79(7), P2–Cu2–I2 = 110.96(5), P2–Cu2–I3 = 104.31(5), P3–Cu2–I2 = 104.31(5), P3–Cu2–I3 = 106.09(5), I2–Cu2–I3 = 102.93(3), P4–Cu3–P5 = 128.58(3), P4–Cu3–I2 = 110.08(5), P4–Cu3–I3 = 101.46(5), P5–Cu3–I2 = 104.36(5), P5–Cu3–I3 = 106.61(5), I2–Cu3–I3 = 103.05(5).

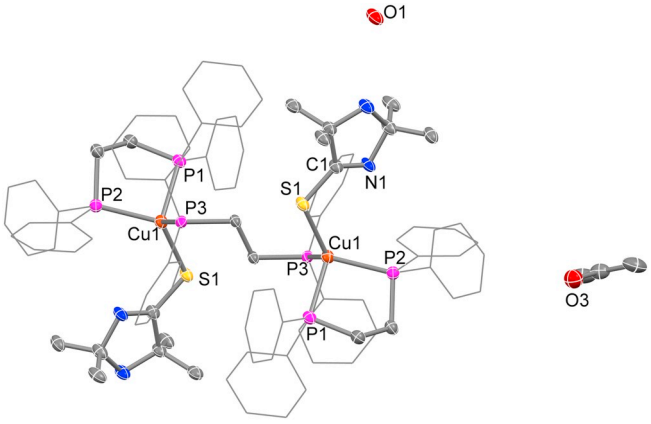

Fig. 4. Crystal structure of compound **4**. Displacement ellipsoids are shown in the 50% probability level. All hydrogen atoms have been omitted for clarity. Selected bond lengths (Å): Cu1–P1 = 2.342(1), Cu1–P2 = 2.284(1), Cu1–P3 = 2.277(1), Cu1–S1 = 2.291(1), S1–C1 = 1.695(4) and bond angles (°): P1–Cu1–P2 = 89.52(5), P1–Cu1–P3 = 108.56(5), P1–Cu1–S1 = 111.89(5), P2–Cu1–P3 = 114.01(5), P2–Cu1–S1 = 118.55(5), P3–Cu1–S1 = 111.90(5), Cu1–S1–C1 = 108.5(1).

Finally, hydrogen bonding interactions between the hydrogen and oxygen atoms of the solvent water molecules belonging to the title and neighboring asymmetric units as well as the protonated amine nitrogen atoms (N2 and N4) of the thiolate groups form an extended network, which expands in space, creating lattice planes nearly parallel to b0c crystallographic plane. This extended rigid hydrogen bonding net concludes a 2D lattice type (Fig. S1), keeping the water solvent and complex molecules together and stabilizing the system.

Table 1
Antimicrobial activity of tmimtH and complexes **1–4** evaluated by minimum inhibitory concentration (MIC) and half-minimum inhibitory concentration (IC_{50}) in μg/mL and in μM (the values in parentheses).

Compound	*E. coli*		*B. subtilis*		*S. aureus*		X. campestris	
	MIC	IC_{50} ± SEM[a]	MIC	IC_{50} ± SEM	MIC	IC_{50} ± SEM	MIC	IC_{50} ± SEM
tmimtH	> 100 (> 631.9)	nd[b]	> 100 (> 631.9)	nd	> 100 (> 631.9)	nd	> 100 (> 631.9)	nd
$[CuCl(\mu\text{-dppe})(tmimtH)]_2$ **(1)**	> 100 (> 76.26)	nd	> 100 (> 76.26)	nd	> 100 (> 76.26)	nd	> 100 (> 76.26)	nd
$[CuBr(\mu\text{-dppe})(tmimtH)]_2$ **(2)**	3.125 (2.23)	1.42 ± 0.065 (1.01)	6.25 (4.46)	2.52 ± 0.017 (1.80)	6.25 (4.46)	5.61 ± 0.016 (4.01)	1.56 (1.11)	1.02 ± 0.008 (0.73)
$[CuI(tmimtH)(\mu\text{-dppe})_2Cu_2I_2(dppe)]$ **(3)**	6.25 (3.25)	3.63 ± 0.023 (1.89)	6.25 (3.25)	3.72 ± 0.016 (1.93)	6.25 (3.25)	4.21 ± 0.008 (2.19)	3.125 (1.62)	1.72 ± 0.012 (0.89)
$[(dppe)(tmimtH)Cu(\mu\text{-dppe})Cu(tmimtH)(dppe)]$ **(4)**	6.25 (3.81)	3.51 ± 0.016 (2.14)	6.25 (3.81)	4.65 ± 0.012 (2.84)	12.5 (7.63)	9.10 ± 0.014 (5.55)	6.25 (3.81)	4.74 ± 0.011 (2.89)

[a] SEM = Standard error of the mean.
[b] nd = not determined.

3.3. Antimicrobial activity

In Table 1, the antimicrobial activities of tmimtH and its complexes **1–4** against two Gram-negative (*X. campestris* and *E. coli*) and two Gram-positive (*B. subtilis* and *S. aureus*) bacterial strains are illustrated. According to our findings, the MIC and IC_{50} values of tmimtH and complex **1** could not be accurately determined due to the restrictions posed by the relatively low solubility and low antimicrobial activity of the compounds. However, this was not the case for complexes **2–4** which apparently possess considerably higher antimicrobial activity than tmimtH. Furthermore, complex **2** exhibited the highest antimicrobial activity against all bacterial strains tested, since it possessed the lowest MIC and IC_{50} values. On the other hand, the two Gram(−) strains (*E. coli* and *X. campestris*) were more susceptible to inhibition of growth by the three compounds for which MIC determination was possible. Regarding the five factors that have been reported to influence the antimicrobial activity of a complex (chelate effect of ligands, nature of ligands, nuclearity, total charge, existence and nature of counterions) [64,65] in the present study the importance of halido ligands is highlighted since this is the main differentiation of the complexes.

3.4. Interaction with CT DNA

Since the compounds exhibit antimicrobial activity, it is necessary to further evaluate their biological activity in order to explore potential biological targets or pathways of mechanisms which are related with antimicrobial activity. Within this context, the interaction of complexes **1–4** with CT DNA was investigated. In most cases, the DNA-interaction of the complexes depends on the structure and stability of the complexes as well as and the nature of their ligands. The interaction of metal complexes with DNA may take place *via* the formation of covalent bonds or in a non-covalent manner (including intercalation, electrostatic interactions and/or groove-binding) or may lead to cleavage of the DNA-helix [66]. In the present study, the interaction of complexes **1–4** with CT DNA was examined by UV–vis spectroscopy, DNA-viscosity measurements and competitive studies with EB (by fluorescence emission spectroscopy).

Titrations monitored by UV–vis spectroscopy are among the most commonly used studies regarding interaction of compounds with DNA. First, the UV–vis spectra of a CT DNA solution were recorded in the presence of the complexes at increasing *r* values. The slight observed changes (increase or decrease) of the absorbance of the DNA-band at λ_{max} = 258 nm (representatively shown for CT DNA in the presence of complex **1** in Fig. 5(A)) may suggest the interaction of the complexes with CT DNA.

Further, the UV–vis spectra of complexes **1–4** were recorded in the presence of increasing amounts of CT DNA and the changes of the intraligand bands located at 271 nm (band I) and 293–298 nm (band II) were monitored. For complexes **1**, **2** and **4**, band I showed a relatively slight hypochromism while band II presented a much more pronounced hypochromism which resulted in the elimination of the band (Fig. 5(B) for complex **1**, Table 2). The addition of CT DNA in a solution of for complex **3** (Fig. 5(C)) resulted in a significant hyperchromism of band I, while band II presented similar behavior as in other complexes (Table 2). In most cases, the observed changes in the UV spectra of the complexes are not as pronounced as to lead to a clear conclusion regarding the possible DNA-interaction mode of the complexes. Subsequently, in order to clarify the DNA-binding mode of the complexes, DNA-viscosity measurements were carried out.

The values of K_b for the complexes were determined by the Wolfe-Shimer equation (Eq. (S1)) [33] and the corresponding plots [DNA]/(ε_A-ε_f) *versus* [DNA] (Fig. S2). The K_b values the complexes (Table 2) are significantly high (of the order $10^5\,M^{-1}$) showing that the complexes are tightly bound to with CT DNA and close or higher than that of the classical intercalator EB ($K_b = 1.23(\pm 0.07) \times 10^5\,M^{-1}$) [67] Concerning the halide X in complexes **1–3**, the K_b constants increase in the order I < Cl < Br, while in the case of the mononuclear Cu(I) complexes with tmimdtH and the phosphines triphenylphosphine or tri-o-tolylphosphine the reported order of K_b-increase was I < Br < Cl [55].

The relative viscosity of a DNA solution (η/η_0) is related to the relative DNA-length (L/L_0) according to the equation $(L/L_0) = (\eta/\eta_0)^{1/3}$, where η_0 and L_0 denote the viscosity and the apparent molecular length in the absence of the compound, respectively [68,69]. Within this context, the changes of DNA-viscosity may be monitored in the presence of a DNA-interacting compound in order to get information regarding this interaction mode, since the presence of compounds: (a) able to intercalate in-between DNA-bases will lead to an increase of the DNA-bases separation distance resulting in increased relative DNA-length and, subsequently, enhanced DNA-viscosity, and (b) that interact with DNA *via* groove-binding or Coulomb forces will induce a bending or/and rotation of DNA helix leading to a slight decrease of relative DNA-length and DNA-viscosity [68].

The changes of relative DNA-viscosity of a CT DNA solution (0.1 mM) were monitored in the presence of increasing amounts of complexes **1–4** (up to the value of r = 0.35). As observed in Fig. 6, the relative DNA-viscosity exhibited an increase in the presence of increasing amounts of complexes **1–4**. Such changes of the relative DNA-viscosity may suggest the possible existence of an intercalative binding mode of the complexes in-between the DNA-bases.

In order to verify the existence of an intercalative binding mode between the complexes and CT DNA, competitive studies with EB were carried out. EB is a typical intercalation marker, since its intercalation to DNA through its planar phenanthridine ring results in the appearance

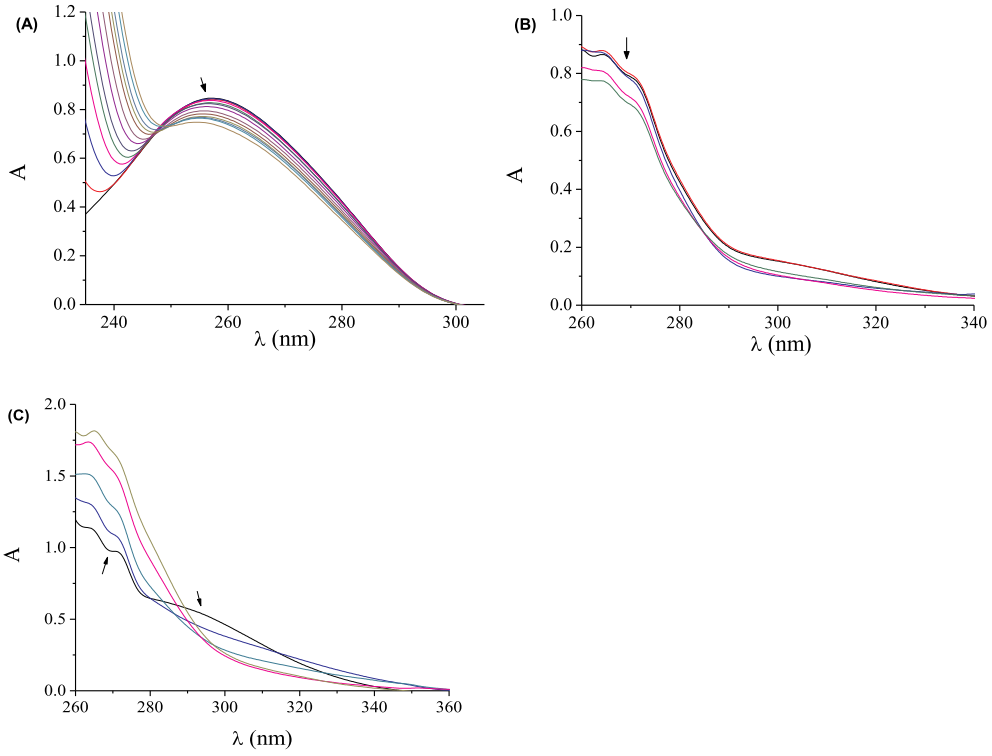

Fig. 5. (A) UV–vis spectra of a buffer solution (15 mM trisodium citrate and 150 mM NaCl at pH 7.0) of CT DNA (1.3×10^{-4} M) in the presence of increasing amounts of complex **1**. The arrow shows the changes upon increasing amounts of the complex. (B)–(C) UV–vis spectra of a DMSO solution of (B) complex **1** (5×10^{-5} M) and (C) complex **3** (1×10^{-4} M), in the presence of increasing amounts of CT DNA. The arrows show the changes upon addition of increasing amounts of CT DNA.

Table 2
UV–vis spectral features of the interaction of the complexes **1–4** with CT-DNA. UV-band (λ, in nm) (percentage of the hyper-/hypo-chromism (ΔA/A_0, in %), blue-/red-shift of λ_{max} (Δλ, in nm)) and DNA-binding constants (K_b, in M^{-1}).

Compound	λ (nm) (ΔA/Ao (%)[a], Δλ (nm)[b])	K_b (M^{-1})
Complex **1**	271 (−10.5, 0); 298 (sh) (−25, elm[c])	$3.20(\pm 0.14) \times 10^5$
Complex **2**	271 (−5, 0)	$4.04(\pm 0.06) \times 10^5$
Complex **3**	271 (> +50, 0); 293 (−35, +6)	$1.04(\pm 0.02) \times 10^5$
Complex **4**	271 (−2.5, 0)	$1.37(\pm 0.18) \times 10^5$

[a] "+" denotes hyperchromism, "-" denotes hypochromism.
[b] "+" denotes red-shift, "-" denotes blue-shift.
[c] "elm" denotes elimination of the band.

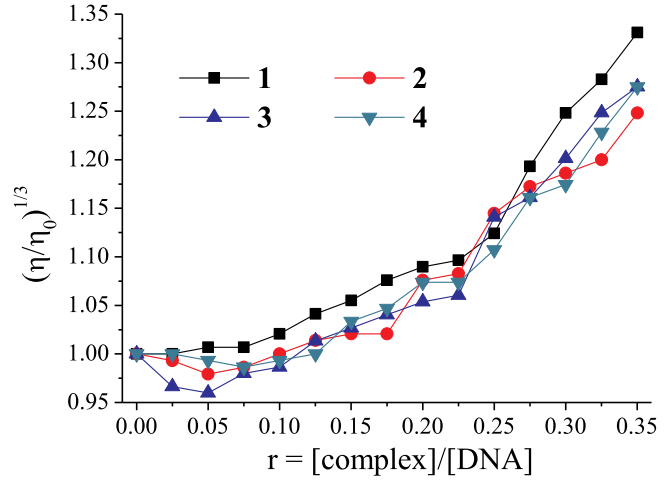

Fig. 6. Relative viscosity $(\eta/\eta_o)^{1/3}$ of CT DNA (0.1 mM) in buffer solution (150 mM NaCl and 15 mM trisodium citrate at pH 7.0) in the presence of complexes **1–4** at increasing amounts (r = [complex] / [DNA]).

of an intense fluorescence emission band at 592 nm, when this EB-DNA conjugate is excited at 540 nm [70]. The addition of a compound which is a candidate intercalator into this solution may result in a competition with EB for the DNA-intercalation sites.

The fluorescence emission spectra of a solution containing EB-DNA which was formed after a 45-min incubation of [EB] = 20 μM and [DNA] = 26 μM were recorded in the absence and presence of the complexes **1–4** (representatively shown for complex **3** in Fig. 7(A)). In the presence of the compounds, the emission band of DNA-EB conjugate at 592 nm exhibited a quenching (the final quenching is up to 71.1% of the initial EB-DNA fluorescence intensity, Fig. 7(B), Table 3), which may reveal the competition of the complexes with EB for DNA-binding sites which may result in a displacement of EB from the DNA-EB conjugate by the complexes and may prove indirectly the probable existence of intercalation of the complexes in-between DNA-bases [34].

The observed EB-DNA fluorescence quenching induced by the complexes is found in good agreement (R = 0.99) with the linear Stern-Volmer equation (Eq. (S2)). The corresponding K_{SV} constants of the complexes (Table 3) were calculated with the corresponding Stern-Volmer plot (Fig. S3) and they are high enough (of the order 10^5 M^{-1}) showing the tight binding of the complexes to the DNA. Furthermore, the calculated (with Eq. (S3)) k_q constants of the complexes (Table 3) are significantly higher than the value of 10^{10} M^{-1} s^{-1} suggesting that the quenching of the EB-DNA fluorescence attributed to the presence of the complexes takes place *via* a static mechanism [34], which further supports the displacement of EB from EB-DNA conjugate.

3.5. Interaction of the compounds with albumins

Serum albumins (SAs), as the most abundant serum proteins, are responsible for various functions including the preservation of osmotic pressure and the transportation of drugs and metal ions towards their biological targets, including cells and tissues [34]. Therefore, monitoring the interaction of SA with potentially bioactive compounds such as complexes **1–4** which have shown antimicrobial activity could be considered a preliminary study to evaluate further the biological activity; upon binding to albumins, the biological profile of the

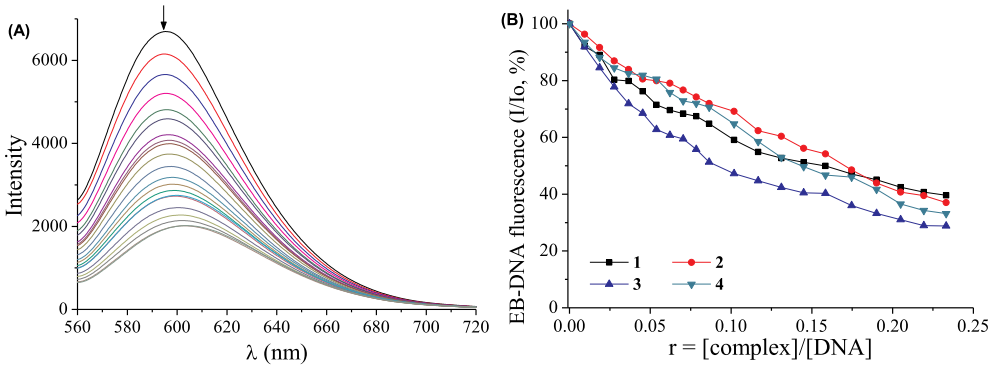

Fig. 7. (A) Fluorescence emission spectra (λ_{exc} = 540 nm) for EB-DNA ([EB] = 20 μM, [DNA] = 26 μM) in buffer solution in the absence and presence of increasing amounts of complex **3** (up to the value of r = 0.24). The arrow shows the changes of intensity upon increasing amounts of **3**. (B) Plot of EB-DNA relative fluorescence intensity (I/Io, %) at λ_{em} = 592 nm *versus* r (r = [complex] / [DNA]) in buffer solution (150 mM NaCl and 15 mM trisodium citrate at pH 7.0) in the presence of complexes **1–4** (up to 39.7% of the initial EB-DNA fluorescence for **1**, 37.0% for **2**, 28.9% for **3** and 33.2% for **4**).

Table 3
Fluorescence features of the EB-displacement studies of complexes **1–4**. Percentage of EB-DNA fluorescence emission quenching (ΔI/Io, in %), Stern-Volmer (K_{SV}, in M^{-1}) and quenching constants (k_q, in $M^{-1}\,s^{-1}$).

Compound	(%)	Ksv (M^{-1})	k_q ($M^{-1}\,s^{-1}$)
Complex **1**	60.3	5.00(± 0.14) × 10^5	2.17(± 0.06) × 10^{13}
Complex **2**	63.0	1.22(± 0.02) × 10^5	5.31(± 0.07) × 10^{12}
Complex **3**	71.1	1.01(± 0.02) × 10^5	4.40(± 0.06) × 10^{12}
Complex **4**	66.8	6.76(± 0.16) × 10^5	2.94(± 0.07) × 10^{13}

compounds may be altered, novel mechanisms of action or transportation may be discovered [71].

The interaction of the complexes with both albumins, *i.e.* HSA and its homologue BSA, was investigated by fluorescence emission spectroscopy. The excitation of the buffer solutions of HSA and BSA at 295 nm results in the appearance of an intense emission band at $\lambda_{em,max}$ = 340 nm and 343 nm, respectively, which is mainly attributed to the existence of tryptophan residues in the albumin, since a tryptophan is located at position 214 in HSA, while the two tryptophan residues of BSA are found at positions 134 and 212.

The quenching of this emission SA-band induced by the presence of complexes **1–4** was low in the case of HSA (the quenching of the initial HSA fluorescence emission (ΔI/Io) was up to ~27% in the presence of **3**, Fig. 8(A)). For BSA, this quenching was enhanced compared to HSA (the quenching of the initial BSA fluorescence emission (ΔI/Io) was up to ~37% in the presence of **2**, Fig. 8(B)). The observed quenching may be attributed to the changes occurring in the environment of SA-tryptophan(s) due to alterations in albumin secondary structure obviously resulting from the binding of the compounds to SAs.

The quenching constants (k_q) of the complexes were calculated from the Stern-Volmer plots (Figs. S4 and S5) and the Stern-Volmer quenching equation (Eqs. (S2) and (S3)), considering as $\tau_o = 10^{-8}$ s the fluorescence lifetime of SA-tryptophan. These k_q values (Table 4) are of the magnitude of $10^{12}\,M^{-1}\,s^{-1}$ and, since they are significantly higher than the value of $10^{10}\,M^{-1}\,s^{-1}$, the existence of a static quenching mechanism may be concluded as a result of the interaction between the compounds and the SAs. Complex **2** shows the highest k_q constants for both albumins among the herein reported compounds.

The SA-binding constants (K) of complexes **1–4** were determined from the Scatchard plots (Figs. S6 and S7) and the Scatchard equation (Eq. (S5)). The K values of complexes **1–4** (Table 4) are in the range 1.11 × 10^4–3.12 × $10^5\,M^{-1}$ and are relatively high enough to show the potency of the complexes to bind to SAs in order to get transported. In addition, the obtained K constants are significantly lower than the value of $10^{15}\,M^{-1}$ (*i.e.* the binding constant of diverse compounds with avidin [72] which is among the strongest known non-covalent reversible interactions [73]); this may suggest that the complexes **1–4** may bind to the albumins reversibly and may get released when they arrive at potential biotargets.

3.6. Docking calculations

Molecular docking calculations were employed to evaluate the ability of compounds **1–4** to bind to macromolecules HSA, BSA, CT DNA and DNA-gyrase, in order to explain the different *in vitro* activity of these compounds. Binding energies for the best docking poses of compounds **1–4** with HSA, BSA, DNA-gyrase and CT DNA are shown in Table 5. From these data, it is obvious that compound **2** seems to succeed better binding (lower binding energy) for HSA, followed by compounds **3**, **4** and **1**. For both CT DNA and DNA-gyrase targets, compound **1** presented better binding followed by compounds **2**, **3** and **4** (DNA-gyrase) and **2**, **4** and **3** (CT DNA). For BSA, lower binding energy was calculated for compound **3** followed by compounds **2**, **1**, and **4**. These data may in part explain the observed *in vitro* activities of the compounds.

The computational approach revealed that all compounds **1–4** are anchored in a cavity of HSA protein formed by domains II, III and IV between binding sites II, III and IV (Figs. 9 and S8). The secondary structures of HSA and BSA shown with the subdomains color-coded are assigned based on Sugio et al. [74] and Bujacz et al. [40], respectively. All compounds are stabilized inside subdomains IIA, IIB and IIIA in a

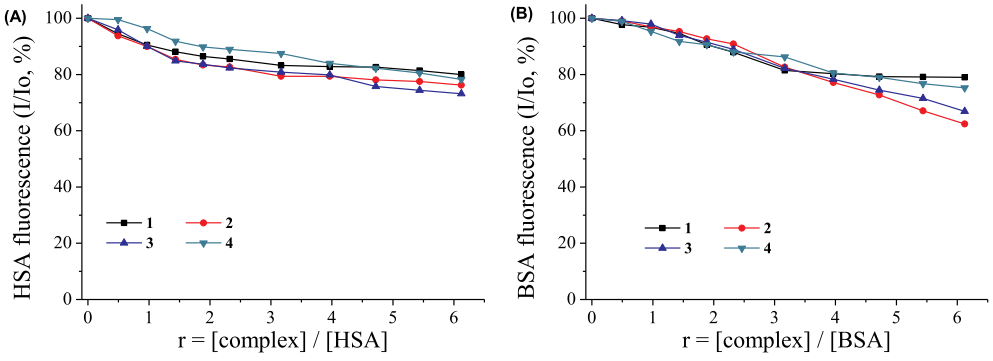

Fig. 8. (A) Plot of relative HSA fluorescence intensity at λ_{em} = 340 nm (I/Io, %) *versus* r (r = [complex] / [HSA]) for complexes **1–4** (up to 80.0% of the initial HSA fluorescence for **1**, 76.2% for **2**, 73.2% for **3** and 78.3% for **4**). (B) Plot of relative BSA fluorescence intensity at λ_{em} = 343 nm (I/Io, %) *versus r* (r = [complex] / [BSA]) for complexes **1–4** (up to 79.0% of the initial BSA fluorescence for **1**, 62.4% for **2**, 66.9% for **3** and 75.2% for **4**).

Table 4
The albumin (HSA/BSA)-quenching (k_q) and binding (K) constants for complexes **1–4**.

Compound	$k_{q(HSA)}$ ($M^{-1}\,s^{-1}$)	$K_{(HSA)}$ (M^{-1})	$k_{q(BSA)}$ ($M^{-1}\,s^{-1}$)	$K_{(BSA)}$ (M^{-1})
Complex **1**	2.51(± 0.21) × 10^{12}	2.01(± 0.10) × 10^5	1.95(± 0.09) × 10^{12}	3.12(± 0.29) × 10^5
Complex **2**	3.17(± 0.22) × 10^{12}	1.68(± 0.06) × 10^5	3.07(± 0.15) × 10^{12}	3.48(± 0.02) × 10^4
Complex **3**	2.06(± 0.07) × 10^{12}	1.21(± 0.06) × 10^5	2.75(± 0.12) × 10^{12}	1.11(± 0.09) × 10^4
Complex **4**	1.49(± 0.05) × 10^{12}	6.55(± 0.37) × 10^4	1.87(± 0.06) × 10^{12}	3.18(± 0.14) × 10^4

Table 5
Global binding energies (in kcal/mol) of complexes **1–4** docked on HSA, BSA, DNA-gyrase and CT DNA targets (PDB accession numbers: 2BXG, 4OR0, 1KZN and 1BNA, respectively).

Compound	HSA	BSA	DNA-gyrase	CT DNA
1	−37.03	−26.32	−50.79	−24.78
2	−56.26	−26.36	−48.64	−23.04
3	−46.90	−28.51	−46.39	−15.69
4	−42.72	−25.09	−30.28	−17.61

pocket formed by a cluster of six a-helices: IIIA-h3, IIIA-h4, IIA-h1, IIA-h2, IIA-h6 and IIB-h9, while for IBP there are depicted two individual poses in the binding sites III and IV. All phenyl rings of dppe moiety participate in hydrophobic interactions, while both imidazolidine rings of tmimdtH moieties participate in both hydrogen bond and hydrophobic interactions. The molecules are anchored in a binding pocket between binding sites II, III and IV and at the same place with the drug iodipamide [39]. Compound **1** is stabilized inside the binding cavity with a hydrogen bond between nitrogen atom of tmimdtH moiety and HND2 or OD1 of Asn295 (3.7 or 3.3 Å, respectively). Asn295 residue therefore assumes a central role in drug interactions. In a close-up view of the ligand-binding pocket of HSA (Fig. 9), is shown that complex **1** is bound in a cavity formed by eleven amino acid residues. Binding interactions of compound **1** with amino acid residues of the binding pocket of HSA are shown in Tables S2. The stabilization of the complex is succeeded with the formation of hydrophobic and polar interactions. Further stabilization of the molecule in the binding pocket is achieved *via* π-π interactions involving the phenyl ring of dppe moiety with imidazole ring of His440 and phenyl ring of Tyr452.

From Tables 4 and 5, it is deduced that complex **2** (which exhibits the highest association constant for BSA) was found also to bind more stable with HSA showing the lowest binding energy (−56.26 kcal/mol). At the same time, for the binding of the complexes on BSA, the order based on association constants are: **2** > **3** > **1** > **4** (complex **4** with the lowest association constant), while from *in silico* prediction **3** > **2** = **1** > **4** (complex **4** again with the highest binding energy, indicating lowest binding capacity with BSA).

The identified drug-binding sites of BSA protein accommodating a number of drugs such as the anticancer drugs doxorubicin and camptothecin (drug-binding site I), warfarin, thyroxin and indomethacin (drug-binding site II), ibuprofen and naproxen (drug-binding site III), ibuprofen, naproxen, halothane, propofol and indoxyl sulfate (drug-binding site IV) and fatty acids, metal ions, dyes and pigments (drug-binding site V) [40] are illustrated in Fig. S9(a). All the simulated binding poses of compounds **1–4** inside the available drug-binding pockets of BSA protein are depicted in Fig. S9(b). Compounds **1** and **2** are anchored in binding pockets of the protein belonging to subdomains IIIB and are positioned in drug-binding site V (with almost the same global binding energy), while **4** is docked in drug-binding site I of subdomain IA. Compound's **3** binding pose inside a pocket of increased volume surrounded by drug-binding sites I, II and IV, formed by subdomains IA, IB, IIA, IIIA and IIIB, is positioned in such a way to make more contacts with the neighboring residues and achieve a better stabilization in the protein structure. The binding interactions of compound **3** in this binding pocket are depicted in Fig. 10. Compound **4** is placed in the same region of the protein where other drug find accommodation, such as the co-crystallized drug NPS, and the important thyroid hormone thyroxine [75]. The stabilization of **3** is succeeded with the formation mostly of hydrophobic interactions, as well as π-π interactions. Our model for BSA complexation with **3** suggests interactions with the dppe moiety of the molecule and only one interaction with tmimtH moiety, probably because of tmimtH's protruding out of the binding cavity. Dppe's and tmimtH's moieties interactions of compound **3** with BSA's amino acid residues are shown in Table S3. The stabilization of the complex is succeeded with the formation of hydrophobic and polar contacts. Additional stabilization is achieved with the inclusion of π-π interactions of phenyl groups with His145 and polar contacts with Lys114 (N, 1.9 Å) and Arg185 (NH2, 2.8 Å). Comparing the binding sites of docked compounds **1–4** in the crystal structures of HSA with the analogous binding sites in the complexes of BSA with the same compounds, it is interesting to observe a distinctive difference in the drug-binding sites, despite the structural similarity between the two proteins. Whereas in HSA all compounds are bound in a pocket formed by subdomains IIA, IIIA and IIB between binding sites II, III and IV, enclosed by helices IIIA-h3, IIIA-h4, IIA-h1, IIA-h2, IIA-h6 and IIB-h9, for BSA a different binding site architecture was revealed. Compounds **1** and **2** are anchored in drug-binding site V or adjacent to this in subdomain IIIB, while compound **3** is stabilized inside a large binding cavity between drug-binding sites I, II and IV, formed by subdomains IA, IB, IIA, IIIA and IIIB, and compound **4** is buried in a pocket in drug-binding site I, adjacent to binding site II, inside the IA subdomain. Compound **1** may be bound more loosely since it protrudes from the cavity mediating less interactions with the protein.

The docking orientations of compounds **1–4** in the crystal structure of CT DNA in the binding cavities of major and minor grooves of DNA are shown in Fig. 11. Compound **1** seems to achieve better stabilization (lower binding energy) inside major groove of DNA due to a hydrogen-bond formed between NH of tmimdtH moiety and OH group of water molecule 51 and a π-π interaction between phenyl ring of dppe with the aromatic rings of nucleotides DA17 and DG16 (Fig. 11). Due to the bulk size of the compounds, they cannot enter the major groove of DNA very deeply as illustrated in Fig. S10. Similar hydrophobic contacts inside the binding pocket of DNA were observed for all compounds, signifying an important role in their stabilization. Ligand-binding site architecture of the docked molecules in CT DNA crystal structure is illustrated in Fig. S11. Interactions of compounds **1–4** with DNA through phenyl carbons of dppe moiety and tmimdtH moiety carbons are shown in Table S4. Compound's **2**C atom of tmimdtH moiety and phenyl C atom of dppe moiety are also interacting with the minor groove of DNA with two polar contacts with the participation of S and O atoms, respectively. Due to shallow penetration of the compounds in major and minor grooves of DNA, no H-bond interruptions between the interstrand nucleotides are observed.

Comparing the DNA binding results (K_b values: **2** > **1** > **4** > **3**), with the *in silico* results (binding energies: **1** > **2** > **4** > **3**), it is obvious that they are in a partial compliance (reverse trend for **1** and **2**). The same is true for comparing the *in vitro* antimicrobial activity (ascending order for MIC and IC_{50} values: **2** > **3** > **4** > **1**) with the computed binding capacity (ascending order for lower binding energies: **1** > **2** > **3** > **4**). An attempt to extract structure activity relationships for the studied compounds **1–4** for their DNA-gyrase

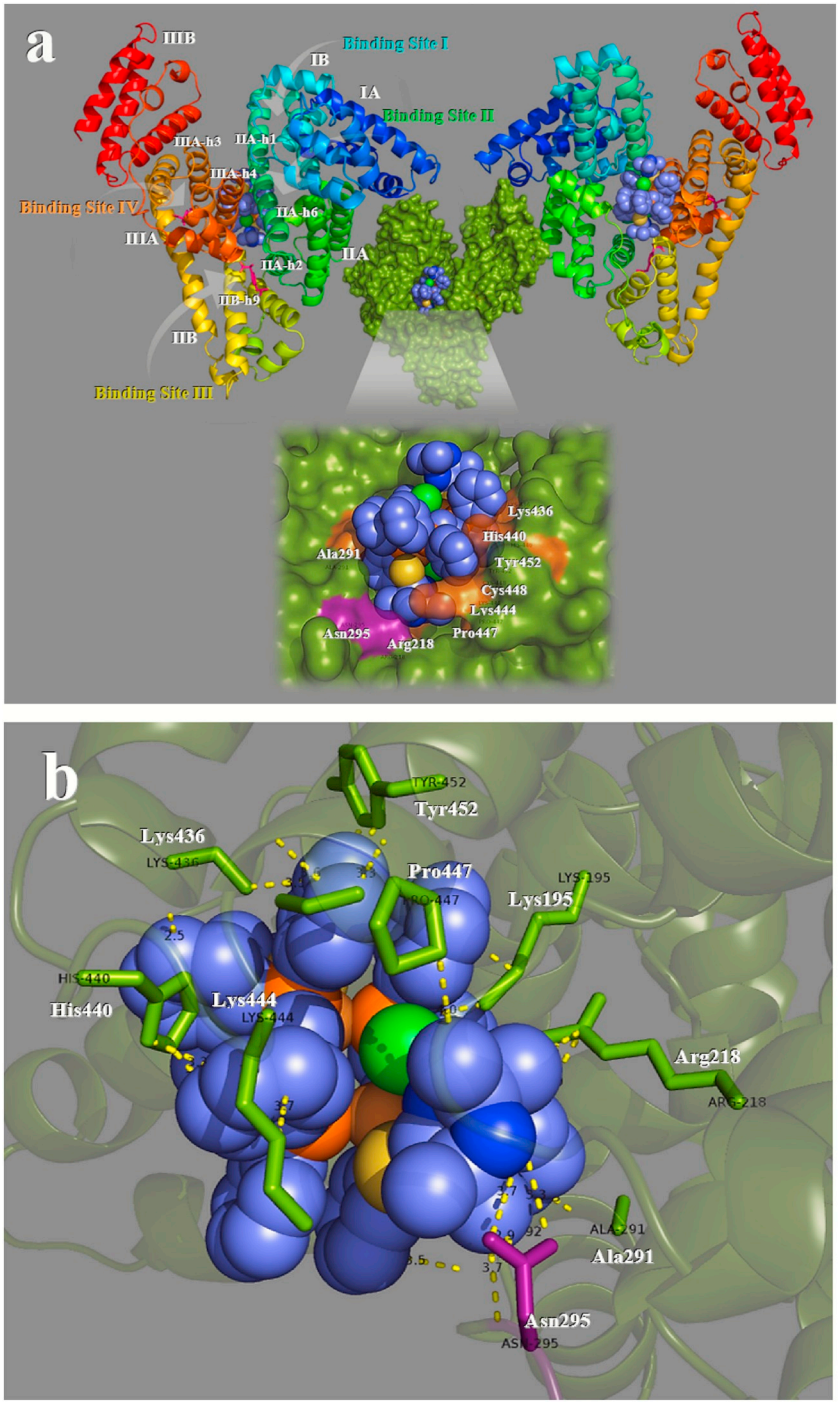

Fig. 9. Molecular docking of compound **1** along with co-crystallized drug IBP into HSA (PDB ID 2BXG) (chain A), depicting the best (lower energy ranking) pose. (a) Target protein is illustrated as cartoon with sub-domains color-coded according to chainbow (left: front view, right: back view). Compound **1** is anchored in a cavity of the protein formed by domains II, III and IV between binding sites II, III and IV. Compound's **1** binding site is enclosed by helices IIIA-h3, IIIA-h4, IIA-h1, IIA-h2, IIA-h6 and IIB-h9, while for IBP there are depicted two individual poses in the binding sites III and IV. Compound **1** is illustrated in sphere representation, while IBP is depicted in stick model. Both molecules are colored according to atom type: slate blue carbon atoms for compound **1** (Cu: brown, Cl: green, P: orange, S: yellow) and hot-pink carbon atoms for IBP. The molecular structure is shown in two orientations for better visibility of its secondary elements. In the right part is shown a 180°-rotated view of the structure revealing the binding pocket of compound **1**. In center part is shown the binding pose of compound **1** (rendered in sphere model with slate blue C atoms) in the protein illustrated as semitransparent surface colored by chain (in splitpea green) with additional depiction of selected contacting amino acid residues of the binding pocket highlighted in magenta for hydrogen bond interaction and orange for hydrophobic and polar contacts. (b) A close up view of the ligand binding site architecture of compound **1** labeled with contacting amino acid residues of the protein illustrated as semitransparent cartoon colored by chain in splitpea green. Yellow dotted lines indicate binding interactions between the docked molecule and the amino acid residues (rendered in stick model and colored in splitpea green) of the binding pocket. Hydrogen atoms are omitted for clarity. Atoms and interacting contacts are numbered according to PyMol software. The final structure was ray-traced. (For interpretation of the references to color in this figure legend, the reader is referred to the web version of this article.)

inhibitory activity reveals that the introduction of halide atoms in the molecular structure of **1–3** contributed in better activity than for a non-halide containing molecule (compound **4**). The observed order of activity is in accordance with the order Cl > Br > I.

We chose to use for docking experiments the DNA-gyrase in complex with bound co-crystallized drug chlorobiocin (CBN) which include only the B subunit exhibiting the crucial ATPase activity (A subunit is mainly involved in DNA breakage and reunion) [76,77].

The best-fitted docking poses of **1–4** inside the ATP-binding site of DNA gyrase protein are shown in Fig. S12. All compounds are shown to be stabilized inside the same binding pocket of the protein occupied by CBN and partially in an adjacent position [41] CBN is one of the most important members of the coumarin family inhibitors of DNA-gyrase activity by competitively binding to the ATP-binding site. The binding pocket is defined by a cavity of approximately 20 Å inside the B subunit of the protein which consists of two domains, an N-terminal domain of ~44 kDa and a C-terminal one of 47 kDa. The N-terminal domain includes two subdomains (24 kDa C-terminal part and 20 kDa N-terminal part). The ATP-binding site is located in the first subdomain of the protein, *i.e.* in the C-terminal part of the N-terminal domain. Compounds **1–4** are shown to lie at the entry of the catalytic pocket partially covering the ATP-binding site. The binding of **1** in the crystal structure of DNA gyrase along with the co-crystallized inhibitor CBN is depicted in Fig. 12. Stabilization of **1** may be attributed to hydrogen bond, polar and hydrophobic contacts inside the ATP-binding site of DNA-gyrase protein (Table S5). Common binding residues with CBN revealed to be Asn46 and Asp45, while the rest residues are sited in adjacent to those of CBN ligand [78,79]. Other key-amino acid residues of the protein's

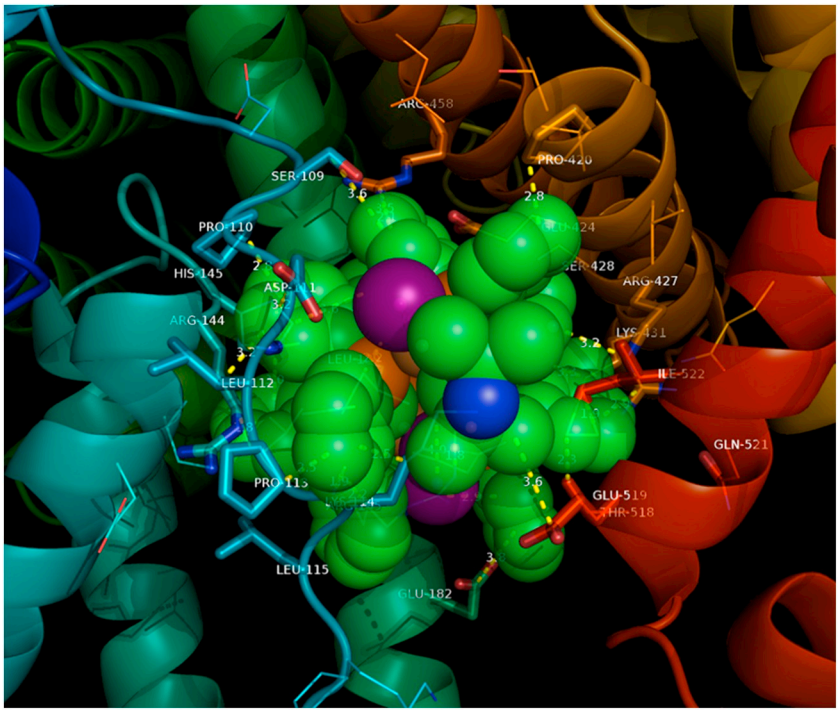

Fig. 10. Docking pose orientation of compound **3** on BSA target protein (PDB ID: 4or0). Compound **3** is docked inside a pocket surrounded by drug-binding sites I, II and IV of the protein and is stabilized with the amino acid residues of the binding cavity (rendered in stick model and colored according to helices coloring). Target protein is illustrated with sub-domains color-coded according to chainbow depicted in depth-cued. Compound **3** is depicted in sphere mode colored according to atom type by green C atoms. Hydrogen atoms of ligand are omitted for clarity. Structure was ray-traced and illustrated with the aid of PyMol Molecular Graphics System. (For interpretation of the references to color in this figure legend, the reader is referred to the web version of this article.)

binding pocket reinforcing the stabilization of compound **1** in the structure are contacts of methyl C of tmimdtH moiety with Gly117 and His116.

4. Concluding remarks

Herein we report the synthesis, solid state crystal structures, as well as the *in vitro* and *in silico* activity of four new copper(I) complexes bearing 1,2-bis(diphenylphosphano)ethane and 2,2,5,5-tetra-methylimidazolidine-4-thione as ligands. The complexes can bind tightly to CT DNA in an intercalative mode as concluded UV–vis spectroscopy and DNA-viscometry studies. The DNA-binding constants are relatively high and the complexes may compete with EB for the DNA-intercalation sites. The complexes may bind tightly and reversibly to serum albumins. *In silico* approaches support the observed *in vitro* data. *In silico* procedures indicate better interaction of compound **2** with HSA, and compound **1** with DNA-gyrase and CT DNA, compared to that of the rest compounds. The results from the present molecular modeling simulations may provide useful complementary insights for the elucidation of the mechanism of action of the studied compounds at a molecular level, contributing to better understanding of both the impairment of DNA by its binding with the studied compounds and also the

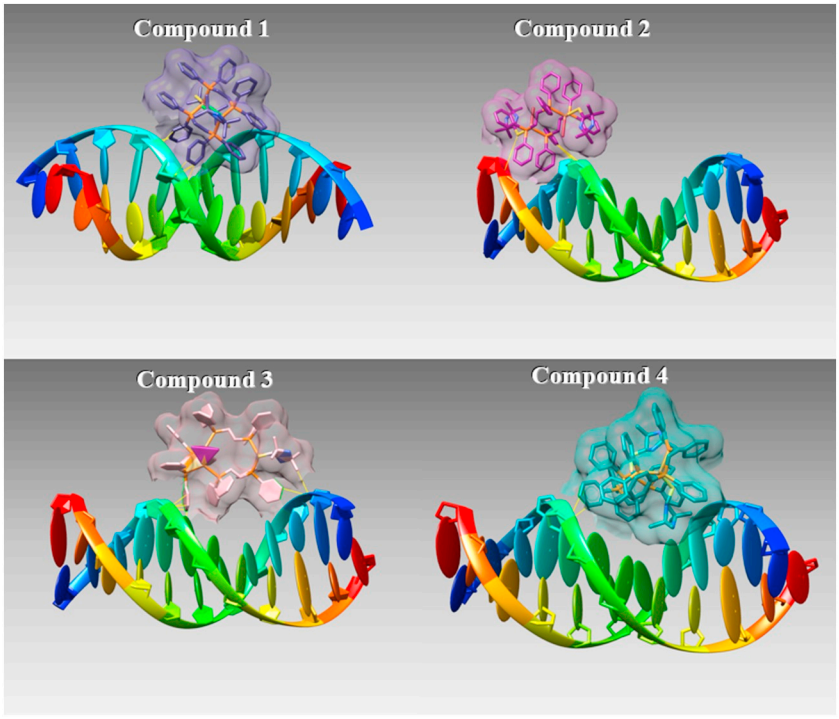

Fig. 11. Molecular docking of studied compounds in the crystal structure of CT DNA (PDB ID 1BNA) in the binding cavity of major groove of DNA for **1**, **3** and **4** and in minor groove for **2**. DNA structure is illustrated with smooth ribbons colored in rainbow, stick bonds, and special representations of the sugars and bases created with the nucleotides extension of UCSF Chimera version 1.11. All compounds are rendered in stick representation and colored according to atom type: magenta, violetpurple, lightpink and deepteal carbon atoms for compound **1**, **2**, **3** and **4**, respectively (Cu: brown, Cl: green, Br: red, I: magenta, P: orange, S: yellow), with a similar color transparent molecular surface. Interacting contacts are shown in yellow lines. (For interpretation of the references to color in this figure legend, the reader is referred to the web version of this article.)

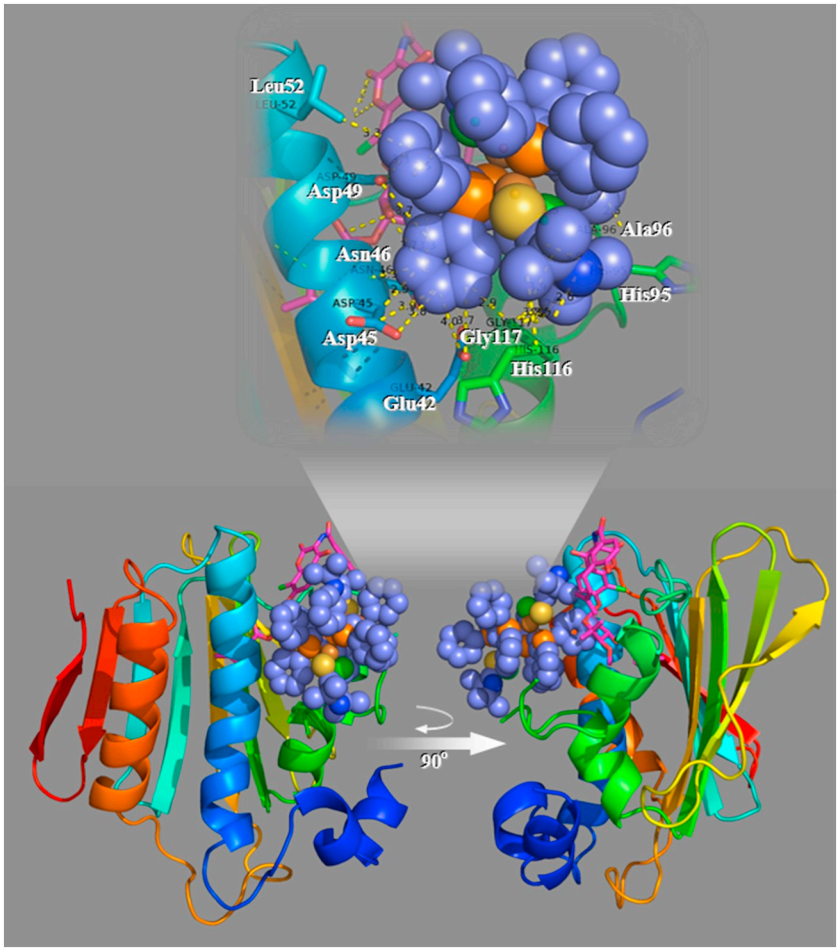

Fig. 12. Molecular docking of **1** illustrated in sphere representation and magenta C atoms (Cu: brown, Cl: green, P: orange, S: yellow) in the crystal structure of DNA-gyrase (PDB ID number: 1KZN), superimposed with the co-crystallized inhibitor CBN (rendered in stick model and hot pink C atoms). On the right side is shown a 90-degree rotated view of the structure. In the model is also depicted the ATP-binding site architecture of the best (lower energy ranking) pose of the compound. Target protein is illustrated as cartoon with sub-domains color-coded according to chainbow. The ligand binding site with additional depiction of selected contacting amino acid residues of the binding pocket is shown in close up view. Hydrogen atoms of all molecules are omitted for clarity. Atoms and interacting contacts are numbered according to PyMol software. The final structure, constructed with PyMol software, was ray-traced. (For interpretation of the references to color in this figure legend, the reader is referred to the web version of this article.)

ability of the compounds for transportation through HSA and possible interaction with other protein targets involved in various diseases.

Abbreviations

B. subtilis	Bacillus subtilis ATCC 6633
BSA	bovine serum albumin
CBN	chlorobiocin
CT	calf-thymus
DMSO	dimethylsulfoxide
dppe	1,2-bis(diphenylphosphano)ethane
E. coli	*Escherichia coli* NCTC 29212
EB	ethidium bromide, 3,8-diamino-5-ethyl-6-phenyl-phenanthridinium bromide
HSA	human serum albumin
IBP	ibuprofen, 2-(4-isobutylphenyl)propionic acid
IC_{50}	half-maximal inhibitory concentration
K	SA-binding constant
K_b	DNA-binding constant
k_q	quenching constant
K_{SV}	Stern-Volmer constant
m	medium
MIC	minimum inhibitory concentration
NPS	naproxen, (*S*)-2-(6-methoxynaphthalen-2-yl)propanoic acid
PDB	Protein Data Bank
r	[compound]/[DNA] ratio or [compound]/[SA] ratio
RCSB	Research Collaboratory for Structural Bioinformatics
RMSD	root-mean squared deviation
s	strong
S. aureus	*Staphylococcus aureus* ATCC 6538
SA	serum albumin
sh	shoulder
tmimdtH	2,2,5,5-tetramethylimidazolidine-4-thione
totp	tri-o-tolylphosphane
vs	very strong
X. campestris	Xanthomonas campestris ATCC 1395
λ_{ex}	excitation wavelength

Appendix A. Supplementary data

CCDC 1903311 - CCDC 1903314 contain the supplementary crystallographic data for compounds **1**, **2**, **3** and **4**, respectively. These data can be obtained free of charge *via* http://www.ccdc.cam.ac.uk/conts/retrieving.html, or from the Cambridge Crystallographic Data Centre, 12 Union Road, Cambridge CB2 1EZ, UK; fax: (+44) 1223-336-033; or e-mail:deposit@ccdc.cam.ac.uk. Supplementary data to this article can be found online at doi:https://doi.org/10.1016/j.jinorgbio.2019.110750.

References

[1] E.S. Raper, Coord. Chem. Rev. 129 (1994) 91–156.
[2] E.S. Raper, Coord. Chem. Rev. 153 (1996) 199–255.
[3] E.S. Raper, Coord. Chem. Rev. 165 (1997) 475–567.
[4] P.J. Cox, A. Kaltzoglou, P. Aslanidis, Inorg. Chim. Acta 359 (2006) 3183–3190 (and references therein).
[5] S.S. Percival, Am. J. Clin. Nutr. 67 (1998) 1064S–10648S suppl. (and references therein).
[6] J.A. García-Horsman, B. Barquera, J. Rumbley, J. Ma, R.B. Gennis, J. Bacteriol. 176 (1994) 5587–5600.
[7] H. Xie, Y.J. Kang, Curr. Med. Chem. 16 (2009) 1304–1314.
[8] Z.H. Chohan, H. Pervez, A. Rauf, A. Scozzafava, C.T. Supuran, J. Enzyme Inhib.

Med. Chem. 17 (2002) 117–122.
[9] D.K. Sau, R.J. Butcher, S. Chaudhuri, N. Saha, Mol. Cell. Biochem. 253 (2003) 21–29.
[10] J.E. Weder, C.T. Dillon, T.W. Hambley, B.J. Kennedy, P.A. Lay, J.R. Biffin, H.L. Regtop, N.M. Davies, Coord. Chem. Rev. 232 (2002) 95–126.
[11] M.R. Moya-Hernández, A. Mederos, S. Domínguez, A. Orlandini, C.A. Ghilardi, F. Cecconi, E. González-Vergara, A. Rojas-Hernández, J. Inorg. Biochem. 95 (2003) 131–140.
[12] K.M. Hindi, M.J. Panzer, C.A. Tessier, C.L. Cannon, W.J. Youngs, Chem. Rev. 109 (2009) 3859–3884.
[13] R.J. Bowen, M. Navarro, A.M. Shearwood, P.C. Healy, B.W. Skelton, A. Filipovska, S.J. Berners-Preis, Dalton Trans. (2009) 10861–10870.
[14] C. Marzano, M. Pellei, F. Tisato, C. Santini, Anti Cancer Agents Med. Chem. 9 (2009) 165–211.
[15] M. Tsiaggali, E.G. Andreadou, A.G. Hatzidimitriou, A.A. Pantazaki, P. Aslanidis, J. Inorg. Biochem. 121 (2013) 121–128.
[16] O. Evangelinou, A.G. Hatzidimitriou, E. Velali, A.A. Pantazaki, N. Voulgarakis, P. Aslanidis, Polyhedron 72 (2014) 122–129.
[17] P.A. Papanikolaou, A.G. Papadopoulos, E.G. Andreadou, A. Hatzidimitriou, P.J. Cox, A.A. Pantazaki, P. Aslanidis, New J. Chem. 39 (2015) 4830–4844.
[18] P. Aslanidis, A.G. Hatzidimitriou, E.G. Andreadou, A.A. Pantazaki, N. Voulgarakis, Mater. Sci. Eng. C 50 (2015) 67–74.
[19] K. Gurova, Futur. Ongology 5 (2009) 1685–1704.
[20] M. Gellert, K. Mizuuchi, M.H. O'Dea, H.A. Nash, Proc. Natl. Acad. Sci. U. S. A. 73 (1976) 3872–3876.
[21] L.L. Shen, D.T.W. Chu, Curr. Pharm. Des. 2 (1996) 195–208.
[22] K.A. Majorek, P.J. Porebski, A. Dayal, M.D. Zimmerman, K. Jablonska, A.J. Stewart, M. Chruszcz, W. Minor, Mol. Immunol. 52 (2012) 174–182.
[23] E.L. Gelamoa, C.H.T.P. Silvab, H. Imasatoa, M. Tabaka, Biochim. Biophys. Acta Protein Struct. Mol. Enzymol. 1594 (2002) 84–99.
[24] G.J. Kubas, Inorg. Synth. 19 (1979) 90–92.
[25] J. Marmur, J. Mol. Biol. 3 (1961) 208–211.
[26] M.F. Reichmann, S.A. Rice, C.A. Thomas, P. Doty, J. Am. Chem. Soc. 76 (1954) 3047–3053.
[27] Bruker Analytical X-ray Systems, Inc., Apex2, Version 2 User Manual, M86-E01078, Madison, WI, (2006).
[28] L. Palatinus, G. Chapuis, J. Appl. Crystallogr. 40 (2007) 786–790.
[29] P.W. Betteridge, J.R. Carruthers, R.I. Cooper, K. Prout, D.J. Watkin, J. Appl. Crystallogr. 36 (2003) 1487.
[30] L.J. Farrugia, J. Appl. Crystallogr. 45 (2012) 849–854.
[31] J.M. Andrews, J. Antimicrob. Chemother. 48 (S1) (2001) 5–16.
[32] E.P. Irgi, G.D. Geromichalos, S. Balala, J. Kljun, S. Kalogiannis, A. Papadopoulos, I. Turel, G. Psomas, RSC Adv. 5 (2015) 36353–36367.
[33] A. Wolfe, G. Shimer, T. Meehan, Biochemistry 26 (1987) 6392–6396.
[34] J.R. Lakowicz, Principles of Fluorescence Spectroscopy, 3rd ed., Plenum Press, New York, 2006.
[35] D.P. Heller, C.L. Greenstock, Biophys. Chem. 50 (1994) 305–312.
[36] L. Stella, A.L. Capodilupo, M. Bietti, Chem. Commun. (2008) 4744–4746.
[37] Y. Wang, H. Zhang, G. Zhang, W. Tao, S. Tang, J. Lumin. 126 (2007) 211–218.
[38] Spartan '08 v.1.1.4, Wavefunction Inc., Irvine, CA, USA; www.wavefun.com.
[39] J. Ghuman, P.A. Zunszain, I. Petitpas, A.A. Bhattacharya, M. Otagiri, S. Curry, J. Mol. Biol. 353 (2005) 38–52.
[40] A. Bujacz, K. Zielinski, B. Sekula, Proteins 82 (2014) 2199–2208.
[41] D. Lafitte, V. Lamour, P.O. Tsvetkov, A.A. Makarov, M. Klich, P. Deprez, D. Moras, Claudette Briand, Robert Gilli, Biochemistry 41 (2002) 7217–7223.
[42] H.R. Drew, R.M. Wing, T. Takano, C. Broka, S. Tanaka, K. Itakura, R.E. Dickerson, Proc. Natl. Acad. Sci. 78 (1981) 2179–2183.
[43] H.M. Berman, J. Westbrook, Z. Feng, G. Gilliland, T.N. Bhat, H. Weissig, I.N. Shindyalov, P.E. Bourne, Nucleic Acids Res. 28 (2000) 235–242.
[44] H.M. Berman, K. Henrick, H. Nakamura, Nat. Struct. Mol. Biol. 10 (2003) 980.
[45] F.C. Bernstein, T.F. Koetzle, G.J. Williams, E.E. Meyer Jr., M.D. Brice, J.R. Rodgers, O. Kennard, T. Shimanouchi, M. Tasumi, J. Mol. Biol. 112 (1977) 535–542.
[46] E.F. Pettersen, T.D. Goddard, C.C. Huang, G.S. Couch, D.M. Greenblatt, E.C. Meng, T.E. Ferrin, J. Comput. Chem. 25 (2004) 1605–1612.
[47] E. Krieger, T. Darden, S. Nabuurs, A. Finkelstein, G. Vriend, Proteins 57 (2004) 678–683.
[48] W.L. DeLano, The PyMOL Molecular Graphics System 0.99, DeLano Scientific, San Carlos, CA, USA, 2006.
[49] P. Viswanathamurthi, M. Muthukumav, J. Chem. Sci. 123 (2011) 567–576.
[50] P. Aslanidis, P.J. Cox, S. Divanidis, P. Karagiannidis, Inorg. Chim. Acta 357 (2004) 4231–4239.
[51] A.A. Del Paggio, D.R. McMillin, Inorg. Chem. 22 (1983) 691–692.
[52] C. Kutal, Coord. Chem. Rev. 99 (1990) 213–252.
[53] D. Anastasiadou, G. Psomas, M. Lalia-Kantouri, A.G. Hatzidimitriou, P. Aslanidis, Mater. Sci. Eng. C 68 (2016) 241–250.
[54] P.J. Cox, P. Aslanidis, P. Karagiannidis, Polyhedron 19 (2000) 1615–1620.
[55] V. Stylidou, K. Kavaratzi, I. Papazoglou, A.G. Hatzidimitriou, A.G. Papadopoulos, P. Angaridis, P. Aslanidis, Eur. J. Inorg. Chem. (25) (2018) 2915–2926.
[56] E.W. Ainscough, E.N. Baker, A.G. Binghan, A.M. Brodie, C.A. Smith, J. Chem. Soc. Dalton Trans. (1989) 2167–2171.
[57] R. Castro, J. Romero, J.A. Garcia-Vazquez, A. Sousa, Y.D. Chang, J. Zubieta, Inorg. Chim. Acta 345 (1996) 119–122.
[58] L.M. Nguyen, M.E. Dellinger, J.T. Lee, R.A. Quinlan, A.L. Rheingold, R.D. Pike, Inorg. Chim. Acta 358 (2005) 1331–1336.
[59] R. Langer, M. Yadav, B. Weinert, D. Fenske, O. Fuhr, Eur. J. Inorg. Chem. (2013) 3623–3631.
[60] A. Sousa-Pedrares, M.L. Durán-Carril, J. Romero, J.A. García-Vásquez, A. Sousa, Inorg. Chim. Acta 263 (2010) 1212–1221.
[61] D. Saravanabharathi, P. Venugopalan Monika, A.G. Samuelson, Polyhedron 21 (2002) 2433–2443.
[62] S.J. Berners-Price, R.K. Johnson, C.K. Mirabelli, L.F. Faucette, F.L. McCabe, P.J. Sadler, Inorg. Chem. 26 (1987) 3383–3387.
[63] P. Comba, C. Katsichtis, B. Nuber, H. Pritzkow, Eur. J. Inorg. Chem. (1999) 777–783.
[64] A.D. Russel, S.S. Block (Ed.), Disinfection, Sterilization and Preventation, fourth ed., Lea and Febinger, Philadelphia, 1991, pp. 27–59.
[65] H.W. Rossmore, S.S. Block (Ed.), Disinfection, Sterilization and Preventation, fourth ed., Lea and Febinger, Philadelphia, 1991, pp. 290–321.
[66] B.M. Zeglis, V.C. Pierre, J.K. Barton, Chem. Commun. (2007) 4565–4579.
[67] A. Dimitrakopoulou, C. Dendrinou-Samara, A.A. Pantazaki, M. Alexiou, E. Nordlander, D.P. Kessissoglou, J. Inorg. Biochem. 102 (2008) 618–628.
[68] D. Li, J. Tian, W. Gu, X. Liu, S. Yan, J. Inorg. Biochem. 104 (2010) 171–179.
[69] J.L. Garcia-Gimenez, M. Gonzalez-Alvarez, M. Liu-Gonzalez, B. Macias, J. Borras, G. Alzuet, J. Inorg. Biochem. 103 (2009) 923–934.
[70] W.D. Wilson, L. Ratmeyer, M. Zhao, L. Strekowski, D. Boykin, Biochemistry 32 (1993) 4098–4104.
[71] C. Tan, J. Liu, H. Li, W. Zheng, S. Shi, L. Chen, L. Ji, J. Inorg. Biochem. 102 (2008) 347–358.
[72] O.H. Laitinen, V.P. Hytonen, H.R. Nordlund, M.S. Kulomaa, Cell. Mol. Life Sci. 63 (2006) 2992–3017.
[73] V. Rajendiran, R. Karthik, M. Palaniandavar, H. Stoeckli-Evans, V.S. Periasamy, M.A. Akbarsha, B.S. Srinag, H. Krishnamurthy, Inorg. Chem. 46 (2007) 8208–8221.
[74] S. Sugio, A. Kashima, S. Mochizuki, M. Noda, K. Kobayashi, Protein Eng. 12 (1999) 439–446.
[75] I. Petitpas, C.E. Petersen, C.E. Ha, A.A. Bhattacharya, P.A. Zunszain, J. Ghuman, N.V. Bhagavan, S. Curry, Proc. Natl. Acad. Sci. U. S. A. 100 (2003) 6440–6445.
[76] J.A. Ali, A.P. Jackson, A.J. Howells, A. Maxwell, Biochemistry 32 (1993) 2717–2724.
[77] J.A. Ali, G. Orphanides, A. Maxwell, Biochemistry 34 (1995) 9801–9808.
[78] A.I. Mohamed, Al-S. Shar, K.A. Reem, El-A. Usama, J. Enzyme Inhib. Med. Chem. 28 (2013) 530–538.
[79] M. Brvar, A. Perdih, M. Renko, G. Anderluh, D. Turk, T. Solmajer, J. Med. Chem. 55 (2012) 6413–6426.